Charles University in Prague
Faculty of Mathematics and Physics

DIPLOMA THESIS

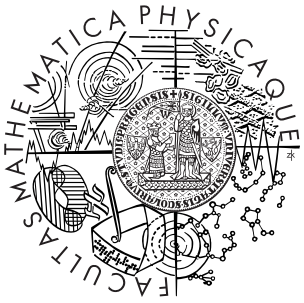

Vlastimil Kůs

Study of diffraction processes at ATLAS experiment

Institute of Particle and Nuclear Physics

Supervisor: Mgr. Marek Taševský, Ph.D

Field of Study: Nuclear and Subnuclear Physics

2009

Acknowledgement: In this place I would like to express many thanks especially to my supervisor Mgr. Marek Tasevsky PhD. for his support, guidance and also patience during work on this thesis. I also would like to thank to Vojtech Juranek and Oldrich Kepka for their valuable advices as well as support in understanding the ATLAS software.
I am very grateful to all other people who supported my work by their help or an advice.

I declare that I wrote my diploma thesis independently and exclusively with the use of the cited sources. I agree with lending and publishing the thesis.

Prohlašuji, že jsem svou diplomovou práci napsal samostatně a výhradně s použitím citovaných pramenů. Souhlasím se zapůjčováním práce a jejím zveřejňováním.

In Prague, 1st August 2009 Vlastimil Kůs

Title: Study of diffraction processes at ATLAS experiment
Author: Vlastimil Kus
Department: Institute of Particle and Nuclear Physics
Supervisor: Mgr. Marek Tasevsky, Ph.D
Supervisor's e-mail address: marek.tasevsky@cern.ch

Abstract: The chapter of forward and diffraction physics is an indispensable and always a rich part of the physics menu of any experiment at high-energy accelerators. In last years, a big effort was put to study and estimate the feasibility or a discovery potential of Higgs boson produced in the central exclusive diffraction events at LHC. These processes have a chance to become competitive or complementary to the program of the Higgs boson search in standard (non-diffraction) processes, in particular in the supersymmetric extension of the Standard model. In this thesis an analysis of the central exclusive production of Higgs boson decaying to two tau leptons is performed, along with investigations of corresponding background processes.

Keywords: diffraction, Higgs boson, forward physics

Název práce: Studium difrakčních procesů na experimentu ATLAS
Autor: Vlastimil Kůs
Katedra (ústav): Ústav částicové a jaderné fyziky
Vedoucí bakalářské práce: Mgr. Marek Taševský, Ph.D
e-mail vedoucího: marek.tasevsky@cern.ch

Abstrakt: Kapitola dopředné a difrakční fyziky je nedílnou a vždy bohatou součástí fyzikálního menu každého experimentu na vysokoenergetických urychlovačích. V posledních letech se značné úsilí věnovalo studiu a odhadu měřitelnosti či objevu Higgsova bosonu v centrálních exklusivních difrakčních procesech na LHC. Tyto procesy mají jistou šanci být konkurencí či doplněním programu pro objev Higgsova bosonu ve standardních (nedifrakčních) procesech, zejména v supersymetrickém rozšíření Standardního modelu. V této práci je provedena analýza centrální exkluzivní produkce Higgsova bosonu rozpadajíciho se v tauonovem kanálu spolu se studiem odpovídajících pozaďových procesů.

Klíčová slova: difrakce, Higgsův boson, dopředná fyzika

Contents

Introduction

One of the most interesting and, at the same time, challenging processes of forward physics are the so called Central Exclusive Diffractive Processes which have recently attracted attention of both theorists and experimentalists. They have unique properties discussed in Chapter 1. In this thesis the central exclusive production of Higgs boson with mass of 120 GeV is studied, along with analyses of background processes. A decay channel of our interest is $H \to \tau\tau$, which has not been studied so far. Although the cross-section of this decay channel is in comparison with other decay possibilities negligible in Standard Model, it seems it could be of some importance within Minimal Supersymmetric Standard Model extension. The point is that we actually do not need high statistics of experimentally discovered events. Only a very few detected events are enough to conclude on quantum numbers of the centrally produced system, in this case Higgs boson. More information is in Chapter 1.

Besides Theoretical introduction in Chapter 1, there is a short overview of a software that has been used for purposes of this analysis (e.g. event generator, detector simulation software and so on), see Chapter 2. In Chapter 3 results concerning exclusive $H \to \tau\tau$ production as well as analyses of background processes are presented. An outlook and a list of remaining points is also mentined. Finally, Chapter 4 presents a summarization of obtained results.

Chapter 1

Theoretical introduction

1.1 Standard Model

In the current particle physics a crucial theoretical framework is the so called Standard Model [1] of elementary particles. It is a quantum field theory involving all fundamental interactions except gravity, i.e. electromagnetic, weak (or unified electroweak) and strong interactions. Although there are sill attempts to include gravity as well, this last interaction remains apart so far, described by Einstein's General Theory of Relativity.

Standard Model, as stated above, is a fundamental theory of elementary particles. By elementary particles we understand point-like constituents of matter with no known substructure so far. There are two basic entities in this theory: particles with half-integer spin (called **fermions**) and those with integer spin (intermediate interaction particles - **bosons**).

Fermions

The elementary fermions are devided into two subgroups: *leptons* and *quarks*. Leptons, carrying a $Q = -1$ charge (in units of e), are electron e^-, muon μ^- and tau τ^-; then corresponding neutrinos are: ν_e, ν_μ, ν_τ. Quarks, carrying fractional charge, are of six different flavors: u (up, 2/3), d (down, $-1/3$), c (charm, 2/3), s (strange, $-1/3$), t (top, 2/3), b (bottom, $-1/3$). Within Standard Model fermions are also organized in three families:

$$\begin{array}{ll} 1^{st} \text{ family:} & \binom{\nu_e}{e^-}, \quad \binom{u}{d} \\ 2^{st} \text{ family:} & \binom{\nu_\mu}{\mu^-}, \quad \binom{c}{s} \\ 3^{st} \text{ family:} & \binom{\nu_\tau}{\tau^-}, \quad \binom{t}{b} \end{array}$$

Quarks are elementary particles carrying an additional quantum number, so called color, of three types. Since the colored objects are not observed

in nature, it is assumed that they are confined into objects (hadrons) in such a way that a resulting particle is colorless. These hadrons are classified into two groups: baryons (made of three quarks) and mesons (made of pairs quark-antiquark).

Bosons

In the Standard Model interactions are described as an exchange of mediating particles - intermediate gauge bosons (spin $s = 1$). For electromagnetic interactions it is only one boson, γ (photon) and is massless, chargeless and nonselfinteracting. Weak interactions, on the other hand, are mediated by 3 bosons, two charged (W^+, W^-) and one neutral (Z^0). They are massive and selfinteracting. Strong interactions among quarks are mediated even by eight bosons, the so called gluons. They are massless, electrically neutral, but carry color, so they can selfinteract.

The three interactions involved in Standard Model have very different ranges, that correspond to a mass of their mediators. The electromagnetic interactions have infinite range (massless photon), the weak interactions have short range (corresponding to massive $W^{\pm}$, Z bosons), around $10^{-16}cm$. On the other hand, strong interactions somehow do not fit into this "mass-model". Their gauge bosons are supposed to be massless but they still have a short range, around $10^{-13}cm$. It is believed to be due to the confinement.

There is one more boson that was not mention yet. It is a cornerstone of the Standard Model (SM), though not experimentally observed yet - a Higgs boson. It is supposed to be a massive (around hundreds GeV) scalar self-interacting particle mediating an interaction of particles with the so called Higgs field. This mechanism was introduced in order to explain the origin of mass of elementary particles as their couplings to a Higgs field. For more information about this topic see e.g. [2, 3].

1.2 Minimal Supersymmetric Standard Model

At present, one of the key problems of particle physics is unraveling the mechanism that breaks the electroweak symmetries and generates the masses of the fundamental particles - electroweak gauge bosons, leptons and quarks (see e.g. [3]). There is a wide range of scenarios extending from weak to strong breaking mechanisms. On one side it is the Standard Model and its supersymmetric extension involving light fundamental Higgs fields, on the other side there are new strong interaction models without the fundamental Higgs field.

The Standard Model requires one complex Higgs field doublet and predicts a single neutral Higgs boson of unknown mass. After extensive searches at LEP (Large Electron-Positron Collider, CERN), a lower bound of 114.4 GeV/c^2 has been established for the mass of the Standard Model Higgs boson, at the 95% confidence level [4]. However, the explanation of electroweak symmetry breaking [5] given in the SM in its minimal form with a single Higgs boson is not considered very satisfactory. Various extended models predict a large diversity of Higgs-like bosons with different masses, couplings and CP-parities. The most elaborated generalization of the Standard Model is its supersymmetric (SUSY) extension called the Minimal Supersymmetric Standard Model (MSSM) (reviewed e.g. in [6]), that requires two Higgs field doublets and predicts the existence of three neutral (h and H are CP-even, A is CP-odd) and two charged (H^+,H^-) Higgs bosons. The lightest of the neutral ones, h, is predicted to have a mass less than about 140 GeV/c^2 and more than about 92 GeV/c^2.

Besides introducing five Higgs bosons, the supersymmetry pairs fermions and bosons, so every Standard Model particle has a counterpart. These supersymmetric partners are supposed to be around hundred to thousand times heavier than proton so a lot of energy is required to produce them. It is expected that supersymmetric particles must be observed at the LHC (Large Hadron Collider, CERN) if they exist. Their interactions and decays are described within MSSM and they have characteristic signatures.

1.3 Decay channels of the Higgs boson

As mentioned in previous sections, Higgs boson as a cornerstone of the Standard Model has been escaping experimental discovery so far. Besides SM (with single Higgs boson), there is several extensions both with and without Higgs boson. In this situation hopes of particle physicists are directed to the LHC collider which has solving of this Higgs or non-Higgs issue among one of its main goals.

A way to discover Higgs boson is through studies of its decays to pairs of fermions or weak bosons. Once we assume a value for its mass (the Standard Model gives no prediction), it is possible to compute rates for its decays into these pairs of particles. In Figure 1.1 there are branching fractions for decay modes that may be promising for the detection of the Higgs boson.

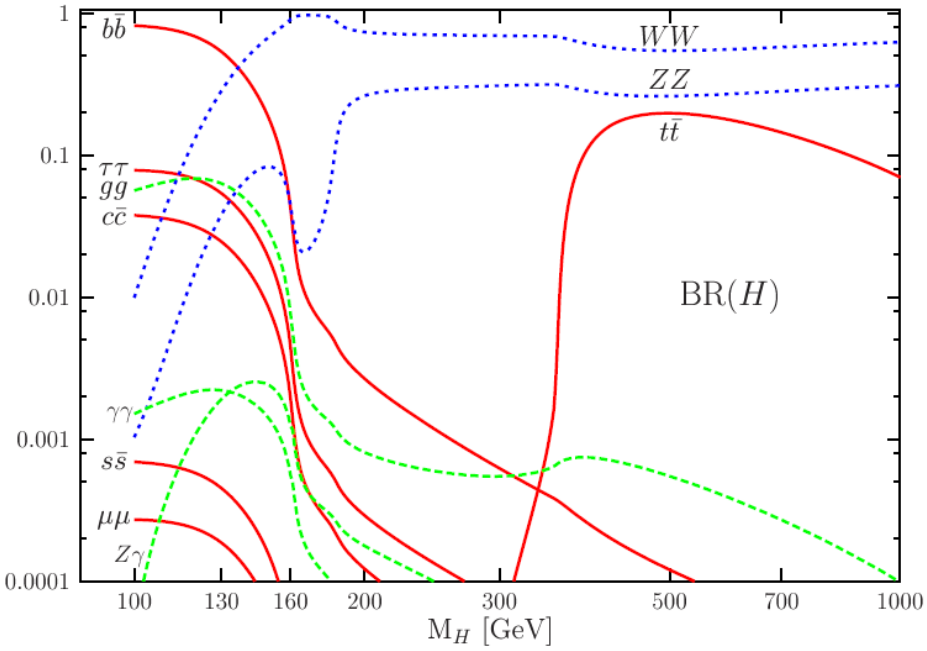

Figure 1.1: Branching ratios for prominent decay modes of the SM Higgs boson; taken from [3].

As we can see from this figure the "strongest" decay channels are $H \to b\bar{b}$ and $H \to WW$. They are discussed some more later in Section 1.8. For now lets just point out that the first one, $b\bar{b}$, is dominant for smaller masses (below about 130 GeV) while the latter one (WW) is dominant for masses

above about 130 GeV. The decay channel of interest for our study is $H \to \tau\tau$. Although it has about one order of magnitude smaller branching ratio, experimental as well as theoretical properties make it very attractive.

The huge QCD-jet backgrounds prevents from detecting the produced Higgs boson (and any particle in general) in fully hadronic modes. When ignoring the light quark and gluon modes, the Higgs boson decays (see Fig. 1.1) mostly into $b\bar{b}$, $\tau\tau$, WW, ZZ and $\gamma\gamma$, $Z\gamma$ final states in the mass range below about 160 GeV and into WW, ZZ and $t\bar{t}$ final states above this mass value. In order to extract a signal in the entire Higgs boson mass range, following requirements have to be met:

- In the WW and ZZ modes, at least one of the W/Z bosons has to be observed in its leptonic decay that has small branching ratios, $\mathrm{BR}(W \to l\nu) \simeq 20\%$ with $l = e, \mu$ and $\mathrm{BR}(Z \to l^+l^-) \simeq 6\%$. In the latter case the invisible neutrino decays, $\mathrm{BR}(Z \to \nu\nu) \simeq 18\%$, can also be sometimes used to increase the statistics. However, a very good detection of isolated high transverse momentum muons and electrons and an accurate calorimetry with hermetic coverage to measure the transverse energy of the missing neutrinos is thus required.

- A very high resolution on photons is necessary to isolate a narrow $\gamma\gamma$ signal peak in the decay $H \to \gamma\gamma$ from the large continuum $\gamma\gamma$ background. Since the Higgs boson width is small, a few MeV for $M_H \simeq$ 120-140 GeV, the measured mass peak is entirely dominated by the experimental resolution. Furthermore, the very large number of high transverse momentum π^0 decaying into two photons, should be rejected efficiently.

- In the dominant Higgs boson decay mode in the low mass range, $b\bar{b}$, excellent microvertex detectors are needed to identify the b-quark jets with a high efficiency and a high purity. τ-lepton identification is also important to detect the decays $H \to \tau^+\tau^-$ and the invariant mass of the final state should be reconstructed with a good resolution.

Beyond the Standard Model the properties of the neutral Higgs bosons can differ drastically from SM expectations, so in case of a discovery of a Higgs boson candidate the immediate other tasks will be making precision measurements of its physical properties and also verifying interpretation of the Higgs boson signal. The separation and identification of different Higgs-like states will be especially challenging. In [11] is shown that the central exclusive diffractive processes (see section 1.5) can play an important role in solving these problems.

1.4 Diffraction - basic concepts

In hadron-hadron scattering a substantial fraction of the total cross section is due to diffractive reactions [7]. These are processes where color singlet objects are exchanged between initial high energy hadrons (protons). Three types of these hadron-hadron diffractive processes are shown in Fig. 1.2: elastic scattering, single dissociation and double dissociation. Except these, multiple Pomeron exchange (and double Pomeron exchange in particular) gives another diffractive events. Anyway, in the of elastic scattering both interacting hadrons emerge intact in the final state, whereas single or double diffractive dissociation corresponds to one or both of them being shattered into a low-mass state. The energy of the final states (either outgoing hadrons or dissociated systems X, Y) is approximately equal to that of the incoming particles (within a few per cents). From Fig. 1.2 we can see, that there is a large gap in rapidity between the two groups of final-state particles (the absence of hadronic activity). This is unique and very useful advantage of these diffractive processes and it will be mentioned later on.

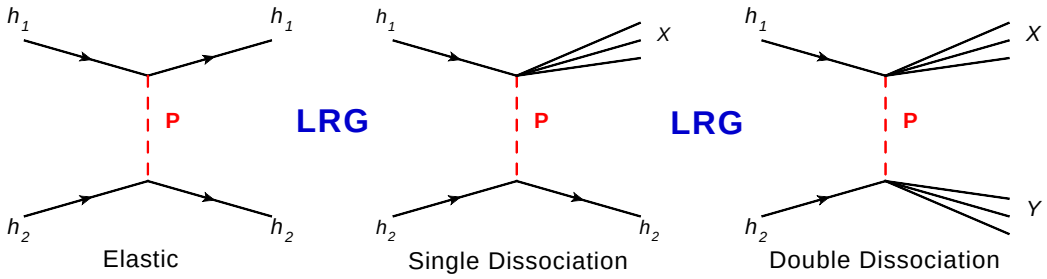

Figure 1.2: Diffractive processes in the collision of two hadrons. Letter P denotes the exchange of a Pomeron in the t-channel, LRG is a shortcut for Large Rapidity Gap (i.e. absence of hadronic activity). There also exist further graphs with multiple Pomeron exchange.

Diffractive hadron-hadron scattering can be described within Regge theory (see e.g. [8]). In this framework, the exchange of particles in the t-channel is summed coherently to give the exchange of so-called "Regge trajectories". Diffraction is characterized by the exchange of a specific trajectory, the "Pomeron", which has the quantum numbers of the vacuum. Regge theory has spawned a successful phenomenology of soft hadron-hadron scattering at high energies. Developed in the 1960s, it predates the theory of the strong interactions, QCD, and is based on general concepts such as dispersion relations. Subsequently it was found that QCD perturbation theory in the high-energy limit can be organized following the general concepts of Regge theory; this framework is often referred to as BFKL [9].

It is clear that a t-channel exchange leading to a large rapidity gap in the final state must carry zero net color: if color were exchanged, the color field would lead to the production of further particles filling any would-be rapidity gap. In QCD, Pomeron exchange is described by the exchange of two interacting gluons with the vacuum quantum numbers.

The effort to understand diffraction in QCD has received a great boost from studies of diffractive events in ep collisions at HERA (see e.g. [10]). One of the essential results of these studies is that many aspects of diffraction are well understood in QCD when a hard scale is present, which allows one to use perturbative techniques and thus to formulate the dynamics in terms of quarks and gluons.

The production of the Higgs boson in diffractive pp collisions is drawing more and more attention as a clean channel to study the properties of a light Higgs boson or even discover it.

1.5 Central exclusive diffractive processes

In the previous section there is a short overview of diffractive processes in particle physics in general. The crucial point is that color singlet objects are exchanged between the high energy initial protons (in the case of LHC). It can occur, for instance, when two gluons are exchanged in the t-channel (this is the case of Higgs boson production studied in this thesis), e.g. as shown in Fig. 1.3. The color is neutralized and allows those two interacting protons to remain intact and just scatter though small angles. Now let's have a look at particular ones, the *central exclusive diffractive processes* (CEDP; see Figure 1.3a), that could play a crucial role in the aim to discover the Higgs boson and to determine its properties.

These processes (see for example [12]) are of the form

$$pp \rightarrow p \oplus \phi \oplus p, \tag{1.1}$$

where the sign $\oplus$ denotes the absence of hadronic activity (so-called 'gap') between the outgoing protons and the decay products of the central system ϕ. These processes have unique advantages as compared to the traditional non-diffractive approaches. Firstly, since the outgoing protons remain intact and scatter through small angles, then, to a very good approximation, the central system ϕ is produced in the $J_z = 0$ (where J_Z is a projection of the total angular momentum of the di-gluon system along the proton beam axis), C and P even state. These properties give a strong suppresion of QCD background. Although an absolute determination of the quantum numbers of any resonance is possible by measurements of the correlations between outgoing protons momenta, the advantage of CEDP is in scattered protons detection - just a few events is enough to determine Higgs boson quantum numbers (0^{++}), contrary to the above mentioned case of measuring correlations (high statistics needed). Secondly, if the forward protons are tagged, then, contrary to a conventional inelastic production, the mass of the produced central system ϕ can be measured to high accuracy by the missing mass method. The equation is

$$M_\phi^2 = s\xi_1\xi_2, \tag{1.2}$$

where s is center-of-mass energy squared and ξ_1, ξ_2 are fractional momentum losses of interacting protons

$$\xi_i = \frac{p_Z^{IN} - p_Z^{OUT}}{p_Z^{IN}} \tag{1.3}$$

(p_Z^{IN} is a proton momentum projection into beam axis before interaction, while p_Z^{OUT} after interaction).

All models for hard diffractive production in central region involve a mixture of perturbative and non-perturbative QCD physics, which is not well understood yet. In Figure 1.3 there is an illustration of three processes for double-diffractive Higgs boson production in hadronic collisions [13].

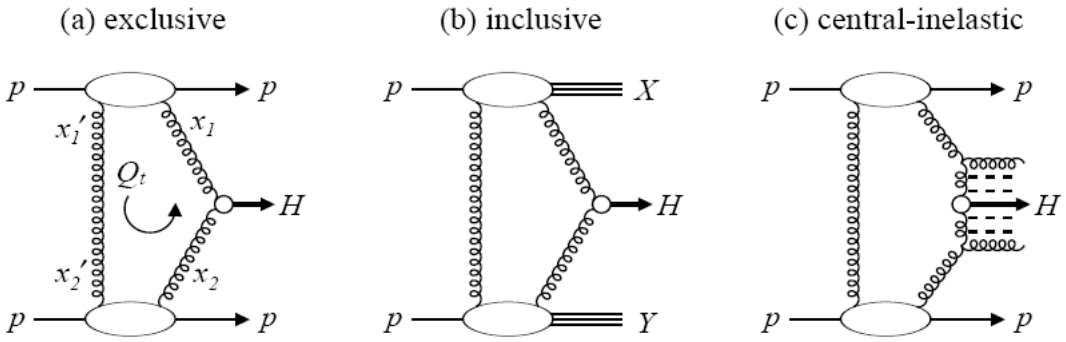

Figure 1.3: Double-diffractive Higgs boson production in pp collisions.; taken from [13].

In the first case, Figure 1.3a, the produced Higgs boson is separated from the outgoing protons by large rapidity gaps. However, this advantage is spoiled for higher luminosities (see chapter about LHC), where the would-be gaps are filled with particles from multiple interactions in bunch crossing (so called pile-up events). The diffractive signature of an event may be, however, recognized by proton tagging in forward detectors. The proton detection is much less dependent on the instantaneous luminosity than the use of large rapidity gaps.

In the Figure 1.3b there is depicted the inclusive process for double-diffractive Higgs boson production. The advantage is much larger cross section, however there is no spin selection rule ($J_Z = 0$) to suppress the $b\bar{b}$ background, so the signal-to-background ratio is unfavourable and the missing mass method cannot be used.

The last depicted process, 1.3c, is a central inelastic production ($pp \rightarrow p + (HX) + p$). There is additional radiation accompanying the Higgs boson in the central region, which is separated from the outgoing protons by rapidity gaps. As in the previous case, neither $J_Z = 0$ selection rule nor the equality of masses measured in forward proton detectors and central detector can be applied, so the signal to background ratio is expected to be very low.

1.6 LHC and its detectors

The Large Hadron Collider (LHC) is located at CERN, near Geneva (Switzerland). It is supposed to start operations in the end of 2009, at reduced luminosities and energies first. It is designed to collide beams of protons and Pb ions, protons at centre-of-mass energy 14 TeV. Protons will be collected in 2808 bunches, each of them about 1.15 x 10^{11} particles, and those will be smashing together every 25 ns (frequency 40 MHz). At the high luminosity mode ($10^{34} cm^{-2} s^{-1}$) it is expected that around 23 overlapping hadronic interactions per bunch crossing will occur.

One of the key characteristics of colliders is their luminosity. It is a factor of proportionality between number of events generated per second N_{events} and cross section σ_{events}

$$N_{events} = L\sigma_{events}. \tag{1.4}$$

There are six detectors for physics studies around interaction points. Two of them are large, ATLAS (A Toroidal LHC ApparatuS) and CMS (Compact Muon Solenoid), designed for luminosities $10^{34} cm^{-2} s^{-1}$ (high luminosity experiments) in proton operation. The other ones are smaller and more specialized. It is LHCb (LHC beauty) designed for luminosity $10^{32} cm^{-2} s^{-1}$ and TOTEM (for detection of protons from elastic scattering at small angles; it shares interaction point with CMS) designed for $L = 10^{29} cm^{-2} s^{-1}$. One experiment at LHC is dedicated to ion experiments: ALICE (A Large Ion Collider Experiment), designed for $L = 10^{27} cm^{-2} s^{-1}$ for Pb-Pb operation. And finally there is LHCf (LHC forward), that shares interaction point (IP) with ATLAS.

TOTEM experiment (Total Cross Section, Elastic Scattering and Diffraction Dissociation) is designed to measure the total and elastic pp cross sections and the diffraction dissociation. It will use two telescopes to detect inelastic events and three so called Roman Pots (RP), that are designed to measure protons scattered under very small angles (defined with respect to the beam axis). The RP detectors in general allow us to measure protons' momenta and so they can be used to determine the mass of the centrally produced object (by the missing mass method mentioned in section 1.5).

1.7 AFP project

AFP (ATLAS Forward Physics) is an upgrade project aiming to install forward proton detectors at 220 m and 420 m from ATLAS interaction point. It offers a rich physics program complementing that of the ATLAS experiment and is supposed to be useful especially in the Higgs boson searches, beyond Standard Model physics, diffraction, QCD and photon-induced processes. The AFP is now under review inside the ATLAS collaboration.

As mentioned in Section 1.5, CEDP are characteristic by the presence of rapidity gaps and nondissociated protons. However, at higher luminosities we cannot rely on gaps since they will be spoiled by soft particles from multiple interactions per bunch crossing (so called pile-up events), so the proton tagging will become preferred option.

There are several location around the ATLAS interaction point at which it is possible to install forward proton tagging detectors. It is 220 m region, where the installation of two sets of Roman Pots [17] (at 216 m and 224 m) is proposed and the 420 m region[1], where are detectors sensitive to lower centrally produced masses (since they are located further away from the interaction point). The acceptance goes down to 100 GeV and decreases rapidly as a function of mass for the 420 m detectors whereas the acceptance of the 220 m pots starts at about 140 GeV. If both protons are detected at 420 m from IP, the missing mass resolution for a 140 GeV central system will be $\sigma \sim 1\%$. If one proton is detected at 220 m and the other at 420 m, the resolution will be approximately 6%. The detectors at 220 m alone can accept only central systems with masses larger than 200 GeV/c^2.

[1]There can't be, however, installed Roman Pots since it is in the cryogenic region of the LHC. The technology for both projects is different.

1.8 CED Higgs boson decays

In the Section 1.3 decay channels of the Standard Model Higgs boson were briefly discussed. Their branching fractions are depicted in Fig. 1.1. Now, since we already know from previous sections about CED (central exclusive diffraction) and its advantages, lets have a look on Higgs boson decays in this case.

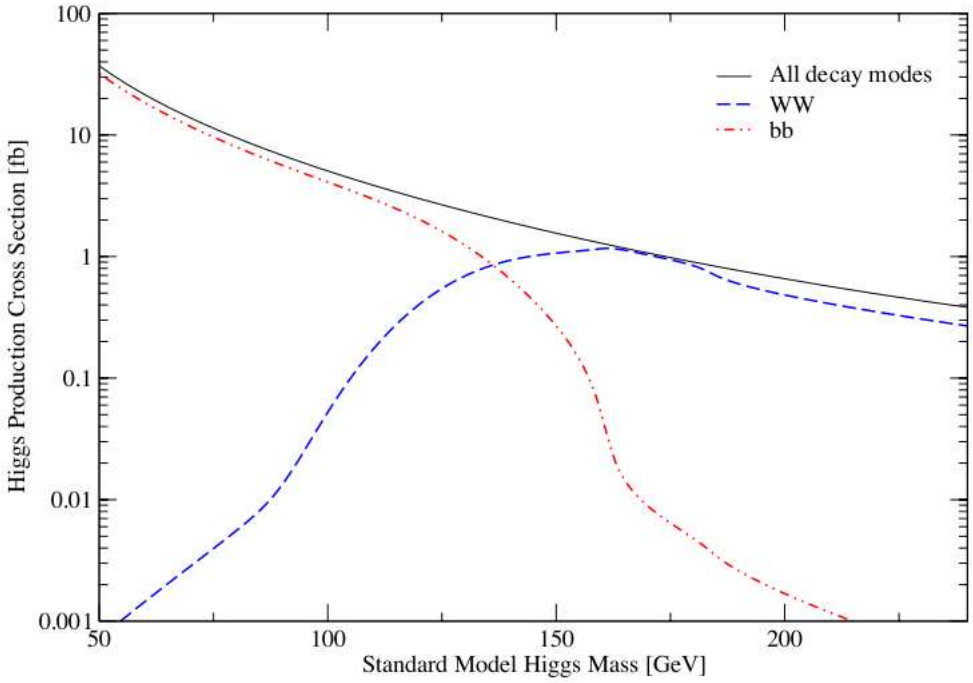

Figure 1.4: Higgs boson production cross section for CED processes; taken from [14].

Figure 1.4 depicts cross section with respect to Higgs boson mass for all decay modes and for $H \rightarrow WW/bb$ separately. We can see that the $b\bar{b}$ is dominant for smaller masses, below around 140 GeV, while WW channel for higher masses, above 140 GeV.

$b\bar{b}$ decay mode

This channel is very attractive for light Higgs boson since it is dominant in that region. However, there are two unpleasantnesses in this process [14]. One of them is b-jet background that is suppressed by the combination of a spin selection rule ($J_Z = 0$) and the mass resolution of proton taggers.

This dependence is an issue since any would-be degradation in the expected resolution will affect the signal to background ratio. This issue also relates to the acceptance-resolution compromise. Lets say we will detect the 120 GeV/c^2 Higgs'. We can choose from two detecting configurations: a combination of 220 and 420 m detectors or both 420 m. While the first one gives reasonable acceptance and a rather moderate resolution, the latter one offers a rather low acceptance but an excellent resolution leading to the efficient background suppression. Another problem worth mentioning is in positions of would-be proton taggers: singals from detectors behind 215 m would arrive too late to the central trigger to be included in its first level.

WW decay mode

The WW mode, however, does not suffer from either of the above problems. Suppression of the dominant backgrounds does not rely primarily on the mass resolution of proton detectors and certainly in the leptonic and semi-leptonic decay channels level 1 triggering is not a problem [14]. From an experimental point of view there are three main categories of WW events. The first one is when at least one W boson decays in either the e or μ channel. These events will usually pass the level 1 trigger thresholds due to the high transverse momentum of the final state lepton. If any of the W bosons does not decay in the e or μ channel there still exists a possibility to pass the level 1 trigger thresholds: it is when W decays in the τ channel (τ decaying leptonically). The last main category of events is the 4-jet decay mode. It occurs approximately half the time, but it is unlikely that it will pass the level 1 triggers without information from proton taggers.

$\tau\tau$ decay mode

There is one decay mode, that has not been mentioned yet: $H \rightarrow \tau\tau$. Unlike the other ones it was not studied closely yet. However, in recent years it is turning out that it could be very interesting process. First, there is practically no irreducible QCD background, although there are other sources of background events (see chapter "Results"). Second, unlike WW or even $b\bar{b}$, events of this type are very "clean", meaning there is only a very few particles per one diffractive pp interaction. As in the WW case, $\tau\tau$ decays can be sorted into three categories. One is *fullyleptonic*, when both taus decay into leptons (electrons or muons); one can also assume that thanks to high p_T of leptons these events will usually pass level 1 trigger. We can also see the exclusivity of these events - there are only two antiparalel leptons with high p_T going into the central detector, nothing more! Another cathegory are

semileptonic events, when there is one τ decaying leptonicly and the other one into hadronic final state. In case both taus are going into hadronic final states we refer to these events as *fullyhadronic*.

Although these events are very specific with respect to their topology and have no QCD background, there is one significant disadvantage: their cross section is about an order of magnitude smaller than even the one of the diffractive $b\bar{b}$. For comparison, see figures 1.4 and 3.1. However, Fig. 3.1 shows Standard Model cross section of $H \rightarrow \tau\tau$. In MSSM, on the other hand, a situation is quite different. There are studies suggesting that *enhancement factors* for MSSM Higgs boson exist, meaning that the actual cross section of this process rises from several unit-times to even several hunderd-times depending on Higgs boson mass and $\tan\beta$ region, as shown in Fig. 1.5. For more elaborate discussion of this topic, see [15].

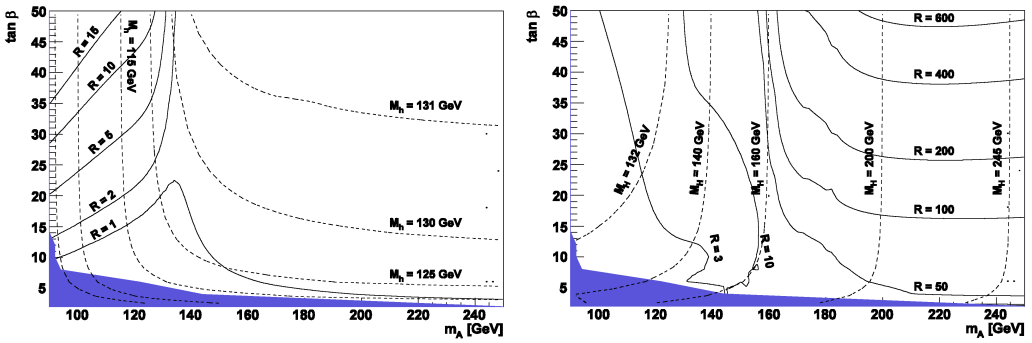

Figure 1.5: Enhancement factors for neutral MSSM Higgs bosons h (left) and H (right). m_A is a mass of the neutral CP-odd MSSM Higgs boson, $\tan\beta$ is a ration of vacuum expectation values of the two Higgs doublets in MSSM; taken from [15].

Chapter 2

Software

2.1 Monte Carlo generators for diffraction

Monte Carlo simulation methods are, in general, a mathematical tools used to solve problems (numerically) that are too complicated to be solved analytically, for example integral calculus. In contrast to other simulation methods, these ones are stochastic (nondeterministic) - their nature is in generating suitable (pseudo-)random numbers. Monte Carlo method is especially effective in solving problems with a large number of degrees of freedom. Its efficiency relative to other numerical methods increases with increasing dimension of the problem.

In nuclear and particle physics (or, more accurately, in processes involving quantum mechanics) a concept of randomness plays a key role in a behaviour of physical systems and Monte Carlo techniques allow us to simulate this randomness. The essential part of event generator is then a random number generator. In practice, however, pseudorandom number generator is used, approximating properties of random numbers.

In section 1.5 there are defined and described central exclusive diffractive processes. At present, there are three Monte Carlo generators that can be used to simulate them: DPEMC [18], EDDE [19] and ExHuME [21]. These models of central exclusive production are either perturbative (ExHuME) or non-perturbative (DPEMC, EDDE).

ExHuME is the Monte Carlo program based on calculation of V. A. Khoze et al. [22], known as Durham Model. This approximation includes a Sudakov factor to suppress radiation into the rapidity gaps and a survival factor, S^2, to ensure that there are no additional interactions between proton lines. The current default value is 0.03 at the LHC.

In contrast, DPEMC and EDDE are non-perturbative models which use the Regge theory (pomeron exchange from each of the proton lines) [8]. DPEMC is based on Bialas-Landshoff approach [23] and it also sets the value of S^2 to 0.03 at the LHC. EDDE uses an improved Regge-eikonal approach [24] and includes a Sudakov suppression factor, but not explicit survival factor.

In each of these Monte Carlos similar available processes are present (e.g. Higgs boson production with all subsequent decays). Di-jet production is also included in all three generators. However, none of Monte Carlos includes next-to-leading order three jet process, which could be very important background to the central exclusive $H \to b\bar{b}$ channel. All three generators give similar predictions for the cross section, but the physics potential decreases for models that include Sudakov suppression, which will limit Higgs boson searches.

2.2 ExHuME generator

In the previous section there are mentioned three Monte Carlo simulation programs used for central exclusive processes. In this section we will focus to one of them, Exclusive Hadronic Monte Carlo Event generator (ExHuME).

In Figure 2.1 there is shown the leading order diagram for central exclusive production, which ExHuME factorises as indicated by the dashed line. In this initial version of ExHuME there are provided $gg \to H$, $gg \to Q\bar{Q}$ (Q is a massive quark) and $gg \to gg$ sub-processes.

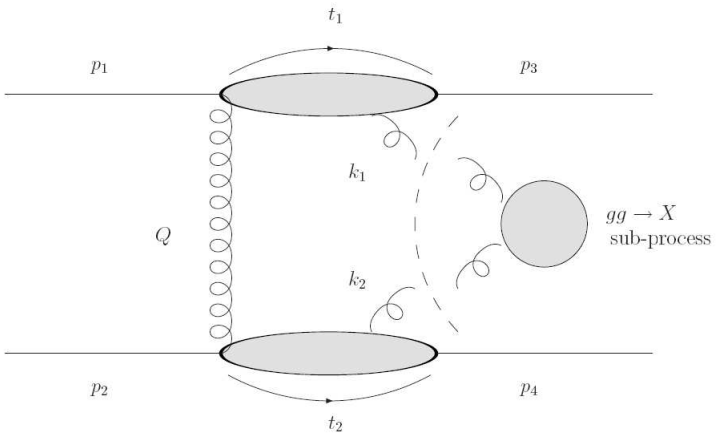

Figure 2.1: The leading order diagram for CEDP of system X; taken from [21].

ExHuME is a C++ program designed to use Pythia [20] for the purposes of hadronisation. Pythia is a program for generation of high-energy events, i.e. for the collisions between elementary particles, in particular interactions in e^+e^-, pp and ep colliders. This event generator contains a wide range of reactions not only within the Standard Model, but beyond it as well (although the physics of processes where strong interactions are involved is not always understood well enough to give an exact description).

ExHuME is written in a C++ object oriented programming language. It includes two main classes: 'CrossSection' class is for calculation of differential luminosity, gluon fusion sub-process and kinematics of outgoing particles and allow us for example to set the decay mode of the Higgs boson; 'Event' class is used for generation of the events and it is able to calculate the total cross section and efficiency of event generation. For comprehensive description of its structure and using see [21].

2.3 ATLAS software

2.3.1 ATHENA

ATHENA [28] is a software framework for ATLAS and is a concrete implementation of an underlying architecture called Gaudi [29] (originally developed by LHCb experiment). Based on GAUDI, ATHENA provides common services such as the transient data store, interactive job configuration and auditing, data access, message streams, etc. for Atlas software. The idea is to improve the coherency of the different software domains within Atlas and thereby the ease of use for end-users and developers, by having them all use the same well-defined interfaces.

2.3.2 Simulation of the ATLAS detector

In order to produce Monte Carlo events on which to perform analysis there is a chain of steps that needs to be taken - it is called the **Full Chain** simulation. It includes four steps: Monte Carlo event **generation**, **simulation** (GEANT4 simulation [30] of the ATLAS detector to produce hits, i.e. a record of where each particle traversed the detector and how much energy etc. was deposited), **digitization** (hits from the simulation are subjected to the response of the detector to produce digits such as times and voltages) and **reconstruction** (raw data digits are reconstructed into tracks and energy deposits).

After going through all the above mentioned steps, the Analysis Object Data (AOD) file, on which a user can perform an analysis, is produced. Because of the time Full Chain takes, especially the Simulation stage, it is expected that most users will not produce many events themselves but will rely on centrally produced events.

2.3.3 Identification of reconstructed particles

In analysis of $H \rightarrow \tau\tau$ we are interested in three reconstructed objects: electrons and muon coming from leptonic decays of tauons and tau-jets coming from hadronic ones. A short overview of used identification procedures is introduced here.

Electrons

Electron reconstruction and identification is ensured by ElectronGamma Combined Performance Group [31]. There are three algorithms used for electron reconstruction. The main one is dedicated mostly to high p_T isolated electrons and it is seeded by a cluster reconstructed in the electromagnetic calorimeter. The second one is dedicated (mostly) to low p_T electrons and electrons in jets. It is seeded by a track in the Inner Detector. The third algorithm is available for the reconstruction of forward electrons. Because of the limited coverage of the tracking system, no trackmatching is required for forward electrons. All algorithms reconstruct the same "Electron" object. An overlap-removal procedure is also applied.

There is a default method for final electron identification, $isEM$ flag. For all electron candidates the candidate has to pass a series of cuts based on the shower shape properties in different compartments of the calorimeter as well as variables combining Inner Detector and Calorimeter information. Three main $isEM$ flag options are Loose, Medium and Tight according to the strictness of a series of cuts. For purposes of the analysis in this thesis **Medium** option has been chosen since it gives reasonable efficiency and small number of fakes (for $H \rightarrow \tau\tau$ events) at the same time.

Muons

Muon reconstruction and identification is ensured by Muon Combined Performance Working Group [32]. It is based on the combined use of data from three subdetectors: Inner Detector, Calorimeters and Muon Spectrometer. There are also many different reconstruction algorithms. For purposes of our analysis standard analysis tools ($AnalysisPreparationTool$, $AnalysisOverlap CheckingTool$ and $AnalysisOverlapRemovalTool$) based on recommended selections from performance groups have been used.

Tau-jets

There are two tau-identification algorithms [33]: $tau1P3P$ and $tauRec$. Although different, they have one feature in common - they are both designed for identification of hadronic tau decays. Originally they were independent, but from recently they were merged together.

The $tau1P3P$ is dedicated for reconstruction and identification of single-prong or three-prong decays (one or three charged hadrons, usually pions, plus arbitrary number of neutral hadrons) with visible energy in the range

from 20 up to 70 GeV. It starts from selecting good quality tracks which provide a seed and requiring low multiplicity of such tracks in the core region of the reconstructed object. The energy of the candidate is calculated with an energy-flow algorithm. Efficient tracking of the Inner Detector and good understanding of the electromagnetic calorimeter is thus crucial. Performance of the hadronic calorimeter is less important, because the energy deposition in the hadronic calorimeter is used only at EM scale for identification quantities and to some extend to guide corrections need for calculating energy scale from energy flow.

The *tauRec* algorithm is based on Calorimeter information. It starts from the cluster reconstructed in the hadronic and electromagnetic calorimeters and then builds a likelihood for the seed to be a hadronically decaying tau, based on 8 different likelihood variables (like number of associated tracks, radius of the cluster in the EM calorimeter and so on). A likelihood is formed to determine how likely a tau candidate originates from a hadronically decaying tau or a QCD jet.

Similarly to the case of electrons, there are $isTau$ flags. This time, however, they are of two kinds: cut-based and likelihood based. Neither of them protects against fake taus coming from electrons and muons - $ElectronVeto$ and $MuonVeto$ flags have to be used in analysis explicitly. Likelihood based thresholds are, similarly to electrons, of three kinds: Loose, Medium and Tight corresponding to 30%, 50%, and 70% efficiency with respect to reconstructed tau candidates. For purposes of our analysis **likelihood Loose** method has been chosen.

Chapter 3

Results

3.1 Introduction to the issue

In Chapter 2, software used for analysis of CEP $H \rightarrow \tau\tau$ is discussed. An overview is certainly appropriate in this place. The analysis goes in subsequent steps:

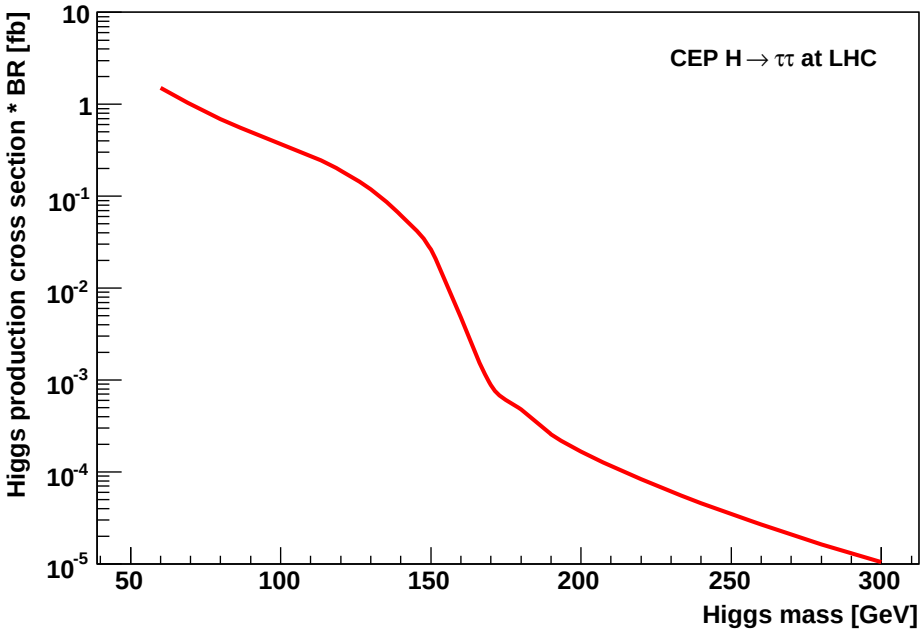

Figure 3.1: CED $H \rightarrow \tau\tau$ cross section.

1. **Generation** - creation of events by the ExHuME Monte Carlo generator (see Section 2.2)

2. **Simulation** - for puposes of our analysis a "Full Chain" simulation of the ATLAS detector running on generated event was used; for more information see Section 2.3.

3. **Analysis itself** - a topic of this chapter

As mentioned before, the central exclusive production of Higgs boson decaying in tauonic channel is the topic of this thesis. A cross section of this process, gained by generating several mass points by ExHuME, is shown in Fig. 3.1. One can see that it is very low even for small masses of Higgs boson. Distinguishing of these events from other sources will be apparently a challenge.

$H \rightarrow \tau\tau$ events can be divided into three cathegories according to final states.

- **Fully-hadronic (hh)** - both taus decaying hadronically
- **Semi-leptonic (hl)** - one tau decaying to electron or muon, the other one decaying hadronically
- **Fully-leptonic (ll)** - both taus decaying to leptons

This naming convention will be used from now on.

As stated in [34] (and confirmed by analysis of our generator-level $H \rightarrow \tau\tau$ samples) the fully-hadronic channel occurs in 43%, semi-leptonic in 45% and fully-leptonic in 12% of events. Hadronic decays of single tau are moreover sorted into two categories: one-prong ($\tau \rightarrow \nu_\tau + h^{\pm}$+n$h^0$) with one charged hadron h occurs in about 77% of tau decays, three-prong ($\tau \rightarrow \nu_\tau$+3$h^{\pm}$+n$h^0$) with three charged hadrons occurs in about 23% of events. Besides charged hadrons there also can be neutral ones. Both charged and neutral hadrons are mostly pions, but also kaons or ρ-mesons are sometimes present.

Unfortunately, triggers have not been studied yet. The idea is to use standard tauonic and leptonic triggers. For the moment we are using following standard kinematical thresholds

- Fully-hadronic cuts:
  $p_T^{jets} \geq 20$ GeV, $|\eta^{jets}| < 2.5$
- Semi-leptonic cuts:
  an electron with p_T>25 GeV or a muon with p_T>20 GeV, all within $|\eta|$ <2.5

- Fully-leptonic cuts:
  $2e(p_T^e$>15 GeV) or $2e(p_{T,max}^e$>25 GeV)
  or $2\mu(p_T^\mu$>10 GeV) or $2\mu(p_{T,max}^\mu$>20 GeV)
  or $e\mu(p_T^e$>15 GeV and p_T^μ>10 GeV)
  or $e\mu(p_T^e$>25 GeV or p_T^μ>20 GeV),
  all within $|\eta|$ <2.5

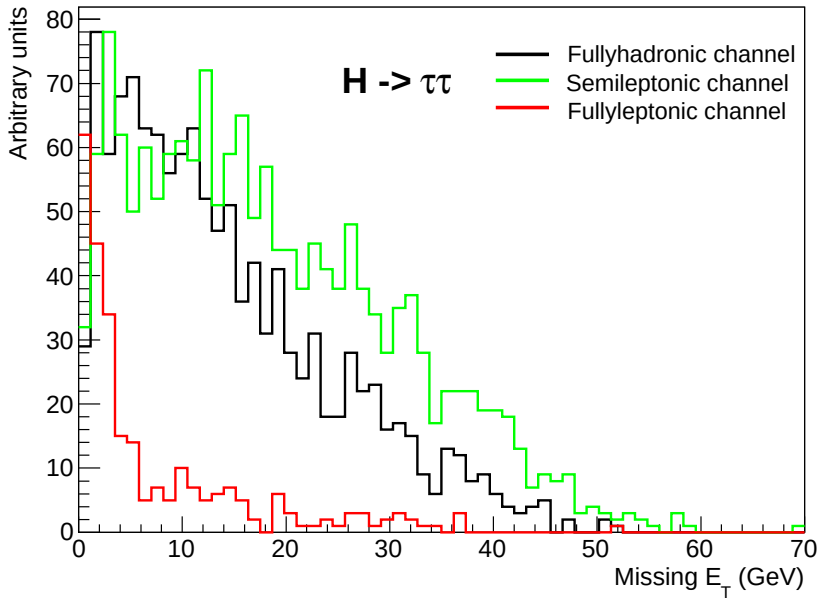

Figure 3.2: Distribution of missing E_T for fully-hadronic, semi-leptonic and fully-leptonic events.

3.2 Study of CED $H \rightarrow \tau\tau$

Unfortunately, there are no ATLAS official production samples of exclusive $H \rightarrow \tau\tau$. Although there was still a possibility to ask for these data, we eventually decided to produce them privately by Full Chain simulation since the current ATLAS production policy requires only 10 TeV center-of-mass energy samples. However, we are interested in 14 TeV samples since this analysis is aimed as a future ATLAS upgrade project, AFP (see Section 1.7). As a future project, all analyses of CED Higgs boson production (ATLAS and CMS analyses as well as theory papers) are based on 14 TeV events.

For the purpose of Full Chain analysis, so called 'job transformations' scripts have been used. By giving them appropriate data and parameters we can go through the whole Full Chain process step by step. As it turned out the choosing of parameters can be tricky. We have eventually decided to run ATLAS simulation under Athena release 14.2.25.10 (see Section 2.3) with ATLAS detector description ATLAS-GEO-02-01-00 and with optional (but for ATLAS-GEO-02-01-00 necessary) job config file '*VertexPos.py*' in GEANT4 step and '*SetJetConstants-02-000.py*' in digitization and reconstruction steps.

3.2.1 Event identification

After Full Chain simulation is successfully finished, the so called AOD file is created. It contains all necessary information such as reconstructed jets, electrons, muons, missing transverse energy, trigger information and so on. On basic level in two-tau events, we are interested in reconstructed electrons, muons and tau-jets. This information is sufficient to determine decay channel, as introduced in previous section. A main part of thi identification algorithm is very straightforward: we require exactly two reconstructed tau-jets for fully-hadronic channel (hh), two reconstructed leptons (electrons or muons) for fully-leptonic channel (ll) and one tau plus one lepton for semi-leptonic channel (hl). Using logical symbols, the logic is as follows:

$$\begin{aligned} \text{hh} &= \text{if(recTaus=2 AND (recElec+recMuon)=0)} \\ \text{hl} &= \text{if(recTaus=1 AND (recElec+recMuon)=1)} \\ \text{ll} &= \text{if(recTaus=0 AND (recElec+recMuon)=2)} \end{aligned}$$

where 'recTaus' corresponds to the number of reconstructed tauons and 'recElec' ('recMuon') to the number of reconstructed electrons (muons).

Needless to say that this algorithm is very strict so some potentially identifiable events are lost. If we sum over all reconstructed tau-jets, electrons and

muons in the particular event, we can introduce a new term: "n-RecLepton event". For example, if $recTaus + recElec + recMuon$ (variables introduced above) is equal to three, we talk about 3-RecLepton events (from the detector point of view). Distribution of n-RecLepton events in case of CEP $H \rightarrow \tau\tau$ is as follows:

$$n_0 = 2341, n_1 = 3965, n_2 = 3030, n_3 = 614, n_4 = 49$$

where n_i are number of i-RecLepton events out of all ten thousands events.

Evidently, the above procedure makes use only of 2-RecLeptons events. One can see that there is also some relevant number of 3-RecLepton events that could make our identification procedure more efficient. However, we have to choose a convenient method to sort them.

There are apparently four cathegories of 3-RecLepton events:

- jjj - three reconstructed tau-jets
- jjl - two tau-jets and one lepton
- jll - one tau-jet and two leptons
- lll - three reconstructed leptons

We get for these cathegories subsequent numbers of events (out of ten thousands simulated ones)

$$jjj = 0,\ jjl = 397,\ jll = 213,\ lll = 4.$$

It is apparent that only jjl and jll possibilities are relevant, i.e. we have to choose between hh and hl channel in jjl case or between hl and ll channel in jll case. The idea is to use standard kinematic cuts on all possible combinations of reconstructed particles and see which combination survives all cuts. This way we are able to sort only around 14% of 3-RecLepton events, but it still makes around 100% improvement in fullyleptonic $H \rightarrow \tau\tau$ decay channel. Numbers of identified 3-RecLepton are

$$hh = 32,\ hl = 25,\ ll = 30$$

There are another 41 overlaps that is not possible to sort this way - both possibilities (either hl and hh in jjl case or hl and ll in jll case) pass kinematic cuts. An idea for sorting remaining overlaps is to use missing E_T information since hh/hl and hl/ll differ by number of escaping neutrinos (the difference is one i both cases), however this turned out to be of no use (see Fig. 3.2).

3.2.2 Basic signatures of exclusive Higgs boson production

Figure 3.3 shows basic distribution plots concerning diffractive protons. Fig. 3.3a contains distribution of p_T^2, 3.3b distribution of proton momentum projection along beam axis, p_Z. We can see that proton p_Z is well peaked in the very vicinity of the original proton energy, 7 TeV. The momentum loss compared to this value is very small, as depicted in Fig. 3.3c (fractional momentum loss ξ is defined in Section 1.5). Finally, Fig. 3.3d shows pseudorapidity distribution of outgoing protons.

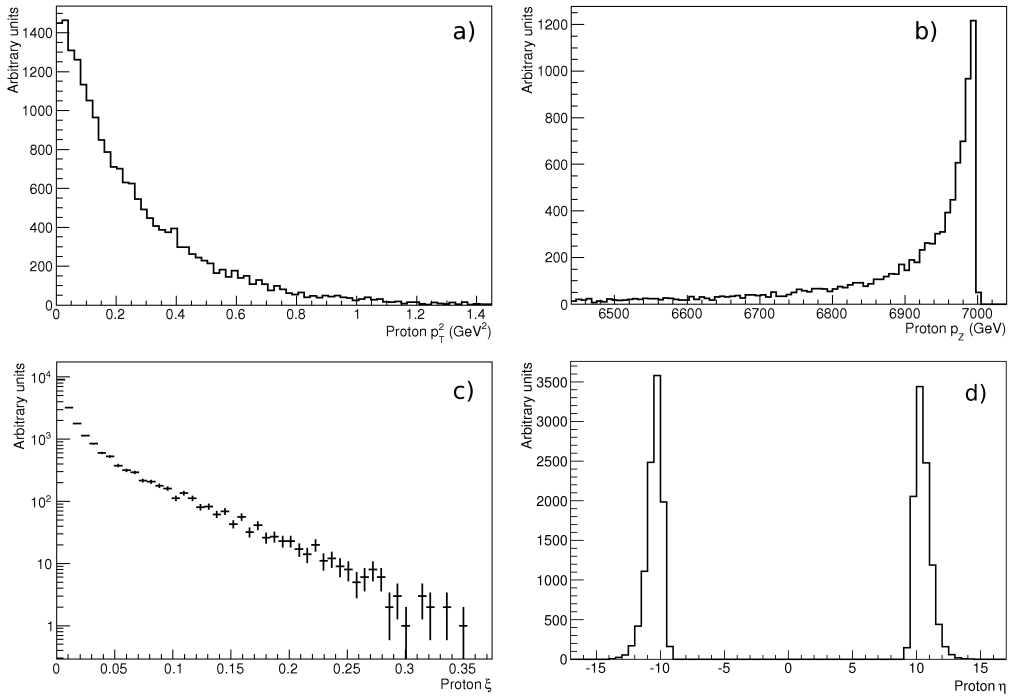

Figure 3.3: Basic distributions of CED protons: a) transverse momentum squared, b) momentum projection to beam axis, c) fractional momentum loss (see Section 1.5), d) pseudorapidity

Other interesting characteristics are those of the produced central system, Higgs boson in this case. We can see them in Fig. 3.4. Fig. 3.4a shows Higgs boson p_T distribution while 3.4b depicts rapidity distribution. One can see that given the mass of our Higgs boson (120 GeV), it stays practically at rest and so we can expect the decay products (two taus) being emitted practically back-to-back.

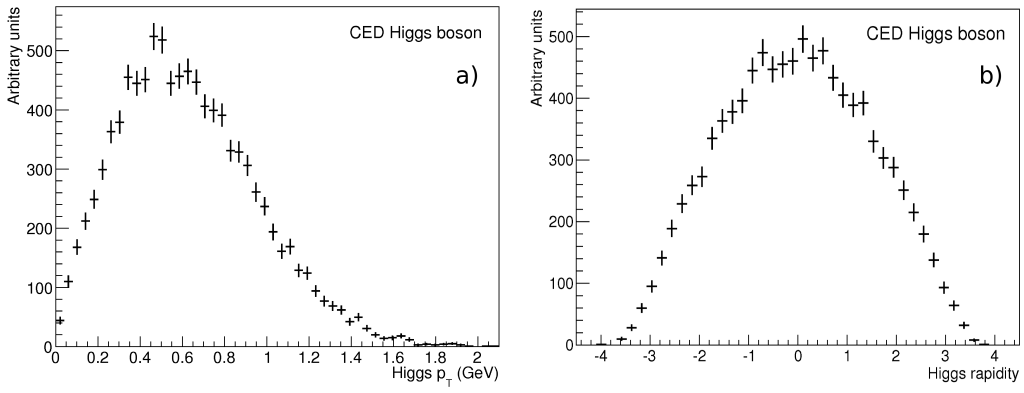

Figure 3.4: Basic distributions of CED Higgs boson: a) transverse momentum, b) rapidity

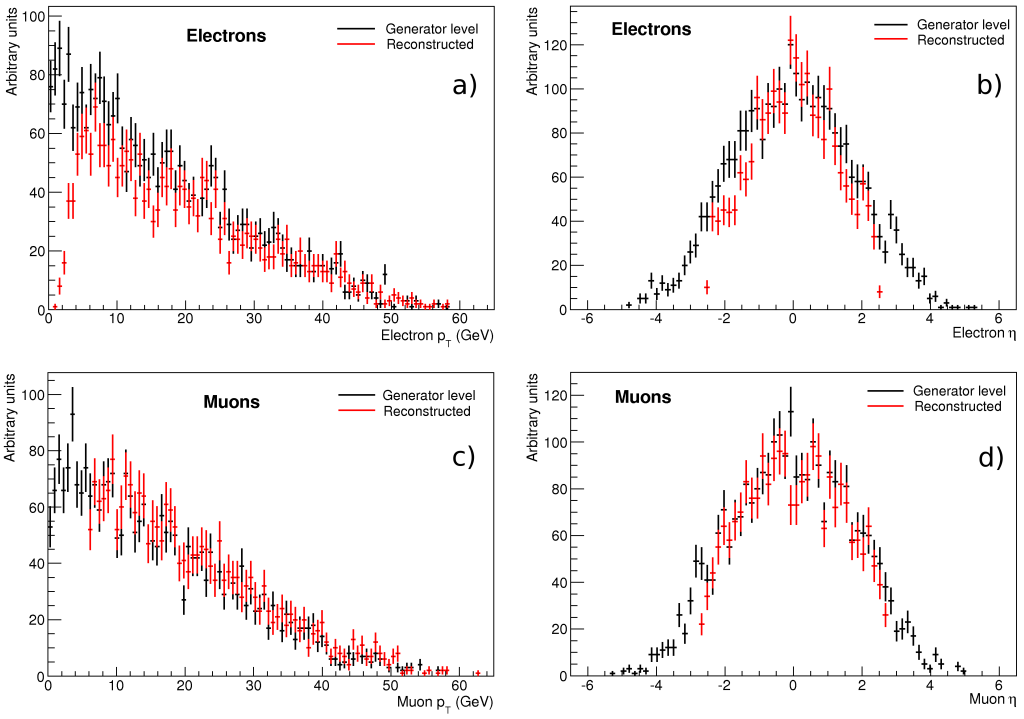

Figure 3.5: Basic distributions of all reconstructed leptons: a) transverse momentum of electrons, b) pseudorapidity of electrons, c) transverse momentum of muons, d) pseudorapidity of muons

3.2.3 Properties of reconstructed leptons

Tau-leptons can decay either into leptonic or hadronic final states. If tauon decays in a hadronic way, we talk about it as 'tau-jet'. In this subsection we will discuss leptonic decays, for tau-jets see next subsection.

Figure 3.5 depicts basic distribution plots of all final reconstructed electrons and muons in comparison with all generator-level electrons and muons. The upper row contains transverse momentum and pseudorapidity of electrons, the lower row of muons. One can see that an efficiency of lepton reconstruction is very good in higher transverse momentum range for both electrons and muons. For transverse momenta below 10 GeV the efficiencies go down. Using the exact numbers, one gets

$$\text{Electrons: } \epsilon = 63\%,\ P = 79\%,$$
$$\text{Muons: } \epsilon = 72\%,\ P = 85\%,$$

where ϵ denotes efficiency (rate of reconstructed electrons/muons out of all generator-level electrons/muons) and P denotes purity (rate of generator-level electrons/muons out of all reconstructed electrons/muons in a particular event). Both values are computed per lepton. It is apparent that not only muon reconstruction is more efficient (about 10%), but it also gives a slightly higher purity.

3.2.4 Properties of reconstructed tau-jets

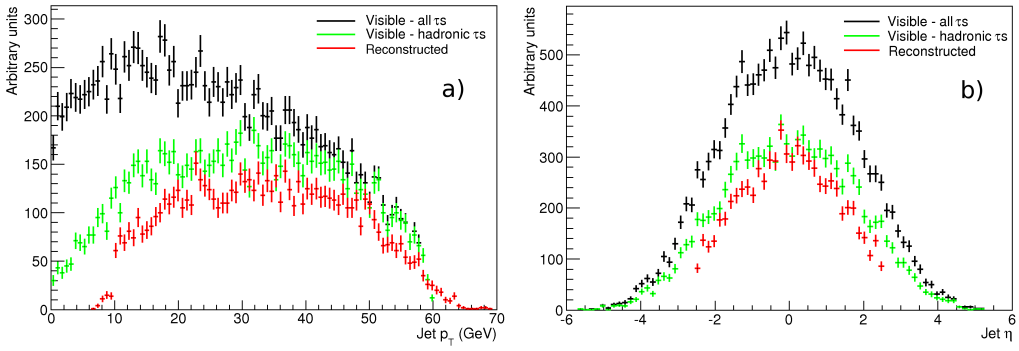

Figure 3.6: Basic distributions of all reconstructed tau-jets: a) transverse momentum, b) pseudorapidity

In Figures 3.6 and 3.7, basic distributions for reconstructed tau-jets are depicted. Also, comparison plots from generator-level are also shown: for hadronic decays of tauons (green lines) as well as for all decays (including leptons; black lines). We can see that tau-jets have, taken in average, higher transverse momenta than those of leptonic decays. This feature is something that can be expected in such decays - in leptonic decay modes there are also other neutrinos except tauonic one carrying out more transverse energy than the one in the hadronic decay. What is important here is that higher energy range of tau-jets means also higher reconstruction efficiency, as shown below.

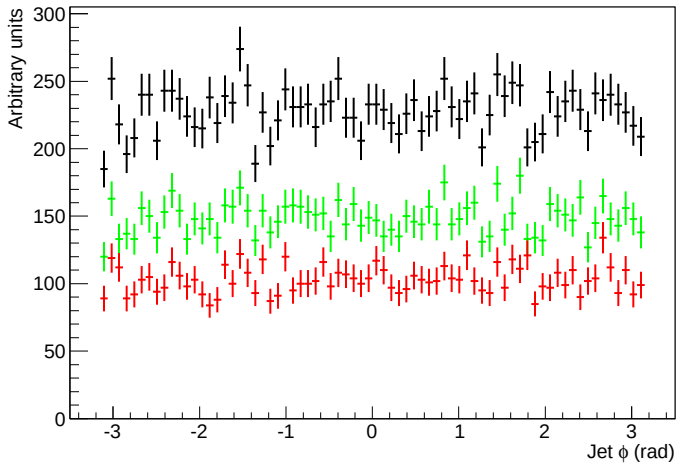

Figure 3.7: Distribution of polar angle of all reconstructed tau-jets.

As mentioned in Section 2.3, the Loose likelihood method is used for final identification of reconstructed tau-jets. There are also two other likelihood

methods - Medium and Tight. According to tau working group (WG) documentation, the efficiencies of tau identification are

$$\begin{gathered}\text{Tight} = 30\%,\\ \text{Medium} = 50\%,\\ \text{Loose} = 70\%.\end{gathered}$$

They are computed with respect to those reconstructed tau candidates that are matched with generator-level tauons decaying hadronically. This computation is carried out by $getTauProngEfficiencies()$ method of $TauValidation$ class (created by tau WG). By the use of this method (with slight modification to our purpose since it is created for computation of cut-based identification methods efficiencies) we get for dataset of official ATLAS production of $Z \to \tau\tau$ events (mc08.106052.PythiaZtautau.recon. AOD.e347_s462_r604_tid038843)

$$\begin{gathered}\text{Tight} = 29.7\%,\\ \text{Medium} = 49.7\%,\\ \text{Loose} = 71.9\%,\end{gathered}$$

which is in an excellent agreement with the official efficiencies above. Finally, for our exclusive $H \to \tau\tau$ samples we get

$$\begin{gathered}\text{Tight} = 57\%,\\ \text{Medium} = 77\%,\\ \text{Loose} = 91\%.\end{gathered}$$

We can see that our efficiencies for $H \to \tau\tau$ are much higher. It is a consequence of different kinematic region. The efficinecies 30%, 50% and 70% were gained from studies of $W \to \tau\nu$ events. In our case, however, we deal with tauons coming from 120 GeV Higgs boson, while the mass of W boson is 80.4 GeV. So our reconstructed tauons have generally higher transverse momentum range resulting in a better reconstruction efficiency.

Last set of histograms illustrating properties of tau-jest is in Fig. 3.8. Distributions a), b) and c) depicts resolution of tau-jets in transverse momentum, pseudorapidity and polar angle. Resolution is defined as

$$R = \frac{X^{Visible} - X^{Jet}}{X^{Visible}} \tag{3.1}$$

where X denotes the examined variable (e.g. transverse momentum), superscript "Visible" denotes a value gained from summing over decay products of the tauon in generator-level and "Jet" denotes a value of reconstructed tau-jet.

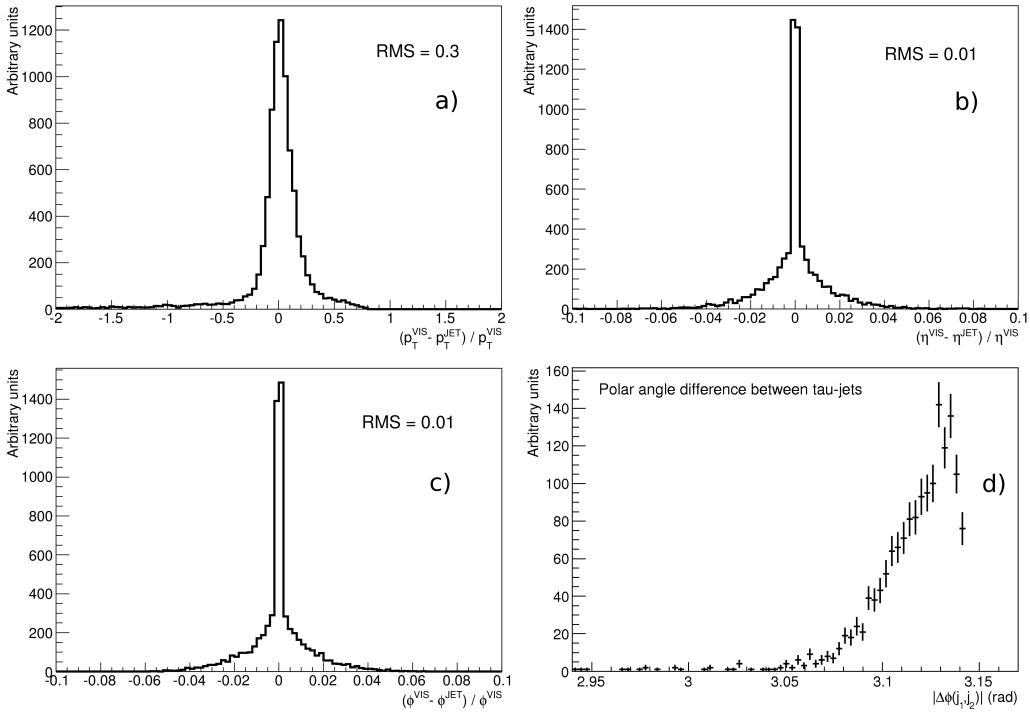

Figure 3.8: Resolutions of tau-jets in transverse momentum (a), pseudorapidity (b) and polar angle (c). Distribution (d) shows polar angle difference between tau-jets.

One can see that these resolutions are very well peaked around zero. For transverse momentum the RMS (root mean squared) is 0.3, for pseudorapidity and polar angle resolutions even 0.01. The fourth plot, Fig. 3.8d, shows the polar angle difference between two reconstructed tau-jets. It is quite narrow and so it could provide a valuable cut for reducing background. We have chosen $3.08 < |\Delta\phi(j_1, j_2)| < 3.15$.

3.2.5 Acceptancies of forward proton taggers, missing mass method

Acceptancies of forward proton taggers

Forward proton detectors, mentioned in Section 1.7, are characterized by their acceptance (efficiency of proton detection) and resolution. Acceptance is a two dimensional function depending on ξ, the fractional longitudinal momentum loss of the outgoing proton and $-t$, the square of four-momentum transfer. It is calculated for both 220m and 420m distances from interaction point and at the low-ξ (i.e. low central masses calculated by missing mass formula, see Eq. 1.2) it critically depends on the distance of the approach of the active area of the detector sensors from the beam. For more details on this subject, see [26]. For purposes of this analysis distances 4mm for 420m and 2.5mm for 220m were chosen. To achieve more realistic beam conditions one also has to smear the beam energy (7 TeV in our analysis) by a Gauss function with $\sigma_E = 0.77$ GeV.

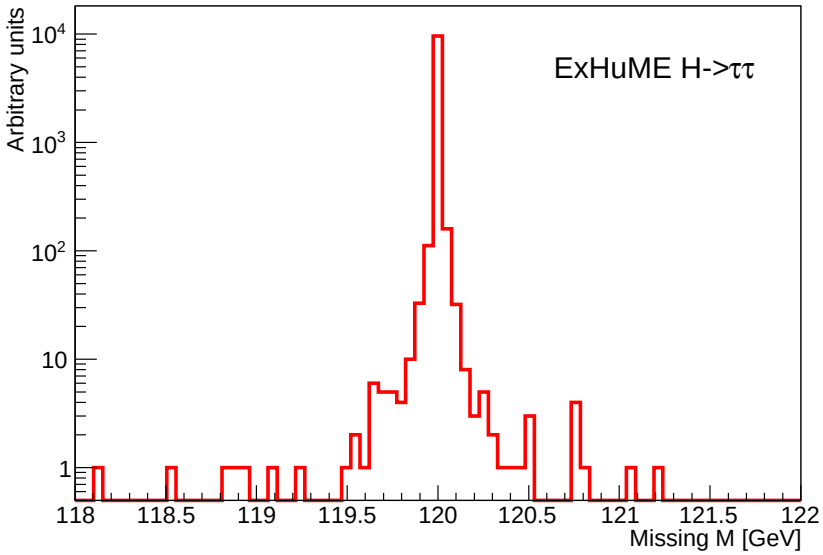

Figure 3.9: Missing mass distribution before any ξ or beam energy smearing. Acceptance taken into account neither. RMS=0.5

Missing mass method

Figure 3.9 shows missing mass distribution without any kind of smearing. No acceptance is taken into account either. On the other hand, plots in Fig. 3.10 depicts the very same distribution, but already with smearing (in both

ξ and beam energy) and with acceptance taken into account. They are fitted by Gauss function with standard deviations

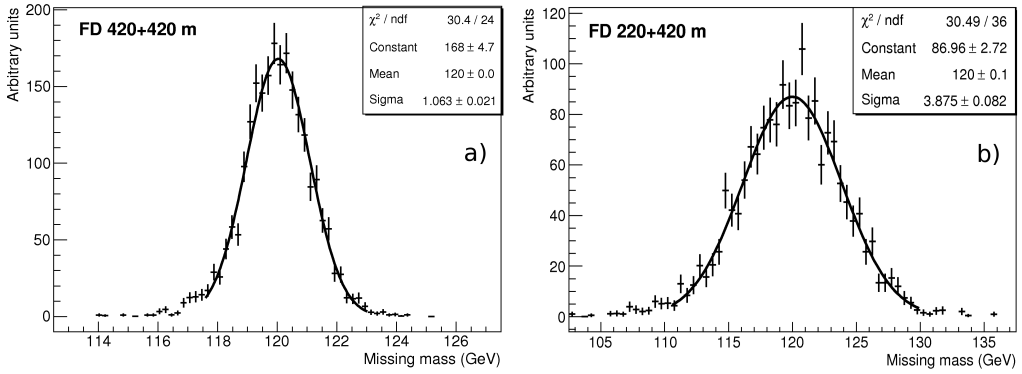

Figure 3.10: Missing mass distributions for two combinations of forward proton detectors: a) 420+420 m, b) both 220+420 m, 420+220 m

$$\text{FD 420+420 m: } 1.1 \pm 0.02 \text{ GeV}$$
$$\text{FD 220+420 m: } 3.9 \pm 0.08 \text{ GeV}$$

Later in this Chapter we will see that cut on missing mass is crucial for suppressing background processes. Given standard deviations above, the missing mass window has been chosen to $\pm\sigma$ corresponding to about 68% surviving signal events. For FD 420+420m we thus get 118.9-121.1 GeV mass window, for FD 220+420m it makes 116.1-123.9 GeV.

Final remark to notation: FD position 220+420 m means both possibilities, 220+420 m (i.e. 220m on a left side and 420m on a right side of the IP) and 420+220 m (i.e. 420m on a left side and 220m on a right side of IP).

3.2.6 Final yields

In Table 3.1 yields of $H \rightarrow \tau\tau$ process cut by cut are presented. Decay channels are denoted according to Section 3.1 as hh, hl and ll. Kinematic cuts on p_T and η (both tau-jets and leptons) correspond to those introduced in the end of the very same Section, "$\Delta\phi(jj)$" is a condition on polar angle distance of two tau-jets (see Section 3.2.4; $3.08 < |\Delta\phi(jj)| < 3.15$), "Mass Window" was introduced in previous section. Finally, "p_T(proton)" is a kinematical cut on both outgoing protons in an attempt to reduce background some more (see next sections). It is set to 200MeV. The keyword "Identified" relates to all events identified (for identification procedure, see Section 3.2.1) as hh, hl or ll with no cuts being applied.

Table 3.1: Yields of $H \rightarrow \tau\tau$ cut by cut.

	FD 420+420 m			**FD 220+420 m**		
Cut	**hh**	**hl**	**ll**	**hh**	**hl**	**ll**
Identified	11.9 %	15.9 %	3.1 %	11.9 %	15.8 %	3.2 %
Acceptance	3.7 %	4.6 %	0.9 %	2.8 %	3.3 %	0.7 %
p_T(lepton)	–	2.0 %	0.7 %	–	1.3 %	0.4 %
η(lepton)	–	2.0 %	0.7 %	–	1.3 %	0.4 %
p_T(jet)	2.9 %	1.9 %	–	2.2 %	1.2 %	–
η(jet)	2.9 %	1.9 %	–	2.2 %	1.2 %	–
$\Delta\phi(jj)$	2.8 %	–	–	2.1 %	–	–
Mass Window	1.8 %	1.3 %	0.5 %	1.4 %	0.8 %	0.3 %
p_T(proton)	**1.4 %**	**0.9 %**	**0.4 %**	**1.1 %**	**0.6 %**	**0.2 %**

We can see that we loose most of events in forward taggers. Their efficiency in 420+420 configuration is 22.9%, for 220+420 configuration it is 17.4%.

In a Tab. 3.2 final yields and corresponding cross-section and absolute numbers of events per 30 inverse femtobarns are presented. Adding both FD 420+420m and 220+420m configurations together we get for final yields of 120 GeV Higgs boson decaying in tau-channel

$$\epsilon = 4.6\ \%, \quad \sigma_{obs} = 8.8\ .\ 10^{-3}\ \text{fb}, \quad N_{ev}/30\text{fb}^{-1} = 0.25.$$

where ϵ is the efficiency after all cuts, σ_{obs} corresponding observed cross-section and N_{ev} absolute number of eventsper 30 fb^{-1}.

It should be stressed here again that this result, i.e. 0.25 events per 30 inverse femtobarns, is related to Standard Model Higgs boson. It was clear from the very begining that $H \rightarrow \tau\tau$ process has no relevant meaning in the SM because of its very low cross-section. This study is, however, aimed at MSSM where enhancement factors are expected (see Section 1.8). In case we

suppose enhancement factor around ten, we can get 2.5 events per 30 fb^{-1}.

A summarization of applied cuts is in order here:

- Fully-hadronic cuts:
  $p_T^{jets} \geq 20$ GeV, $|\eta^{jets}| < 2.5$
  $3.08 < |\Delta\phi(jj)| < 3.15$

- Semi-leptonic cuts:
  an electron with p_T>25 GeV or a muon with p_T>20 GeV, all within $|\eta|$ <2.5
  $p_T^{jet} \geq 20$ GeV, $|\eta^{jet}| < 2.5$

- Fully-leptonic cuts:
  $2e(p_T^e$>15 GeV) or $2e(p_{T,max}^e$>25 GeV)
  or $2\mu(p_T^\mu$>10 GeV) or $2\mu(p_{T,max}^\mu$>20 GeV)
  or $e\mu(p_T^e$>15 GeV and p_T^μ>10 GeV)
  or $e\mu(p_T^e$>25 GeV or p_T^μ>20 GeV),
  all within $|\eta|$ <2.5

For all cases above additional cuts are

Mass Window (FD 420+420m) = 118.9 - 121.1 GeV
Mass Window (FD 220+420m) = 116.1 - 123.9 GeV
p_T(protons) $\geq$ 200 MeV

Table 3.2: Summary of final yields along with corresponding cross-sections and absolute numbers of events per 30 fb^{-1} for $H \to \tau\tau$ events.

Selection cuts	**FD 420+420 m**			**FD 220+420 m**		
	Eff. [%]	σ [fb]	**Events/ 30 fb^{-1}**	**Eff.** [%]	σ [fb]	**Events/ 30 fb^{-1}**
Generated	100 %	0.1899	5.70	100 %	0.1899	5.70
FD acceptance	22.9 %	0.0435	1.30	17.4 %	0.0330	0.99
hh cuts	2.8 %	0.0053	0.16	2.1 %	0.0040	0.12
Mass Window	1.8 %	0.0034	0.10	1.4 %	0.0027	0.08
p_T(protons)	1.4 %	0.0027	0.08	1.1 %	0.0021	0.06
hl cuts	1.9 %	0.0036	0.11	1.2 %	0.0023	0.07
Mass Window	1.3 %	0.0025	0.07	0.8 %	0.0015	0.05
p_T(protons)	0.9 %	0.0017	0.05	0.6 %	0.0011	0.03
ll cuts	0.7 %	0.0013	0.04	0.4 %	0.0008	0.02
Mass Window	0.5 %	0.0009	0.03	0.3 %	0.0006	0.02
p_T(protons)	0.4 %	0.0008	0.02	0.2 %	0.0004	0.01
Overall	**2.7 %**	**0.0052**	**0.15**	**1.9 %**	**0.0036**	**0.10**

3.3 Background studies

As mentioned in theoretical introduction, there is practically no irreducible QCD background to the $H \to \tau\tau$. There are, however, other sources (see [25]).

1. **Exclusive $\gamma\gamma$ fusion** (Fig. 3.11a) producing pairs of leptons (electrons, muons, tauons): $pp \to p + ll + p$

2. **Exclusive production of high E_T gluons**: $pp \to p + gg + p$
   The gluons could be misidentified as a pair of hadronic tauons.

3. **Di-jets + pileup.**
   Overlap of a di-jet event (missidentified as $\tau^+\tau^-$) combined with two single diffractive events (Fig. 3.11b coming from pile-up gives the same event from detector point of view as our signal event.

Unfortunately, there are no official ATLAS samples of events of exclusive $\gamma\gamma$ fusion. The private production, as in CED Higgs boson case, was thus necessary. There exists a generator called FPMC [27] (Forward Physics Monte Carlo) which is designed for this kind of processes. It was used to generate ten thousands events for all three possibilities: $\gamma\gamma \to ee$, $\gamma\gamma \to \mu\mu$ and $\gamma\gamma \to \tau\tau$. These three samples were subsequently submitted to full chain ATLAS detector simulation with ATLAS-GEO-02-01-00 detector description version under Athena release 14.2.25.10 (along with job config files '*VertexPos.py*' and '*SetJetConstants-02-000.py*' as in the $H \to \tau\tau$ case).

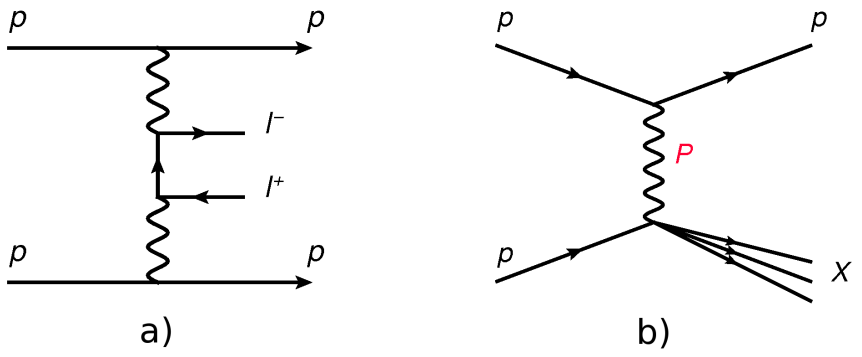

Figure 3.11: Background processes: a) $\gamma\gamma$ fusion producing pair of leptons, b) single diffraction

3.3.1 Exclusive $\gamma\gamma \to e^+e^-$ production

Properties of scattered protons

As in the case of exclusive $H \to \tau\tau$, distributions of basic kinematic variables of scattered protons in exclusive $\gamma\gamma$ fusion events are presented here, see Figure 3.12. For comparison reasons, plots of exclusive $H \to \tau\tau$ events are also depicted here (red lines).

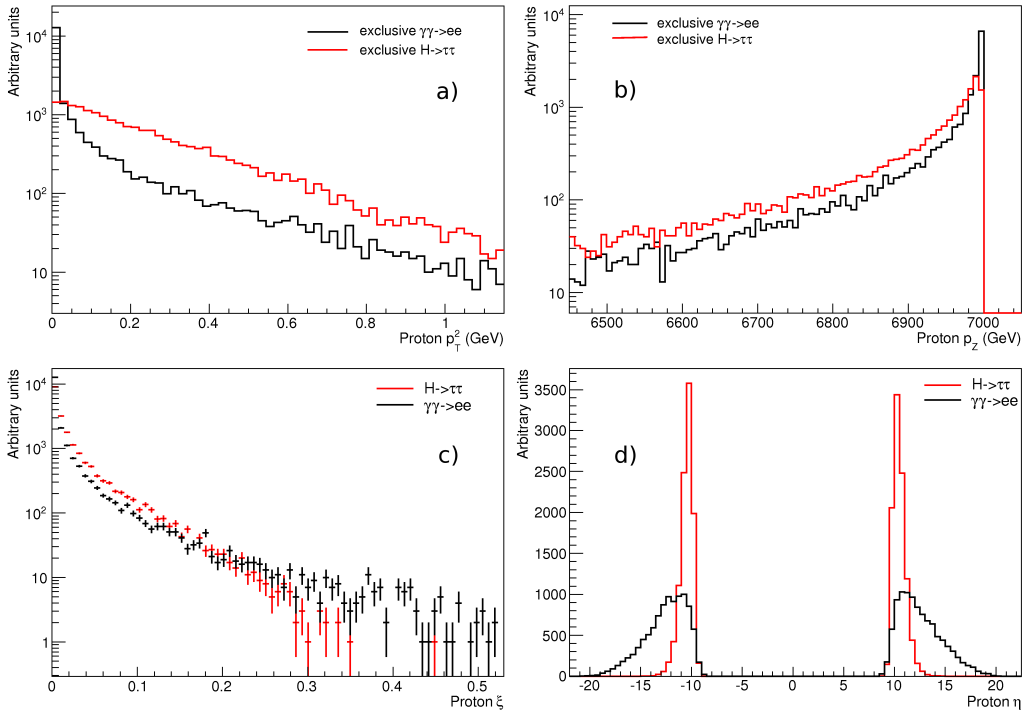

Figure 3.12: Basic distributions of CED protons: a) transverse momentum squared, b) momentum projection to beam axis, c) fractional momentum loss, d) pseudorapidity

As we can see from transverse momentum squared distribution in Fig. 3.12a, a mean value of transverse momentum of the exclusive $\gamma\gamma$ fusion is smaller than that one of the central exclusive diffraction. We can use this feature to our advantage and introduce a p_T cut of a small value (200 MeV) on outgoing protons, which should suppress this background process. What is also worth mentioning are Fig. 3.12b and 3.12d. We can see that the distribution of projection of proton momentum to beam axis is slightly narrower than in the case of exclusive Higgs boson production, while the pseudorapidity distribution (Fig. 3.12d) is on the other hand broader.

As in case of $H \to \tau\tau$, we show here the missing mass distribution with smearing (in both ξ and beam energy) and with acceptance taken into ac-

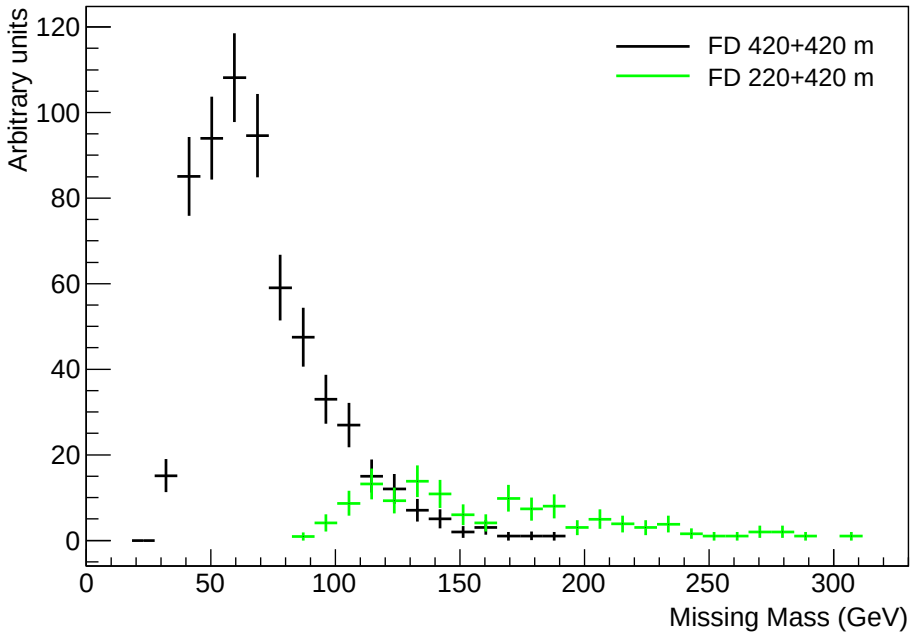

Figure 3.13: Missing mass distribution of exclusive $\gamma\gamma \to ee$ process.

count, see Fig. 3.13. We can see that the appropriate mass window cut will remove most of these background events.

Properties of reconstructed electrons

In Fig. 3.14 transverse momentum and pseudorapidity of reconstructed electrons in comparison with generator-level electrons are shown. Electrons coming from exclusive $\gamma\gamma$ fusion have apparently softer p_T spectrum than in CED $H \to \tau\tau$ case which also means that smaller reconstruction efficiency is to be expected, which is confirmed by actual numbers

$$\epsilon = 52\%,\ P = 62\%,$$

where ϵ denotes efficiency per electron and P is purity per electron (as defined in Section 3.2.3).

Properties of reconstructed tau-jets

Although it can be surprising a bit, there is quite a number of reconstructed tau-jets. In absolute numbers, it is 4024 tau-jets out of ten thousands $\gamma\gamma \to ee$ events. Their transverse momenta and pseudorapidities distributions are in Fig. 3.15. Again, we can see that these tau-jets have much softer p_T

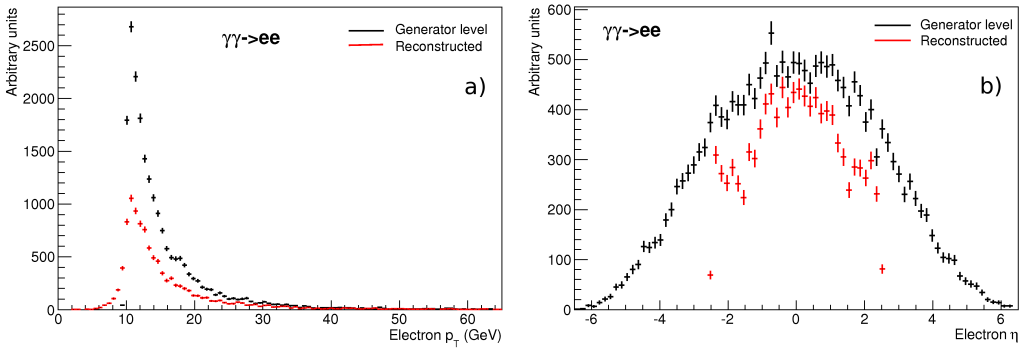

Figure 3.14: Distributions of reconstructed (red lines) and generator-level (black lines) electrons: a) transverse momentum, b) pseudorapidity

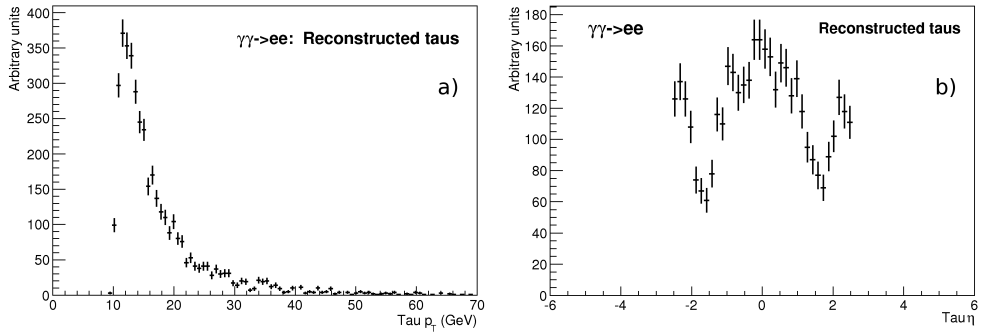

Figure 3.15: Distributions of reconstructed tau-jets: a) transverse momentum, b) pseudorapidity

spectrum. Anyway, such an number of identified tau-jets in purely electron-electron events suggests that distinguishing electrons from tauons can be an issue. Electrons leave one charged track in the Inner detector and cause an electromagnetic shower in the calorimeter. Majority of tauons decaying into hadronic final state is 1-prong (i.e. having only one charged particle), 77% to be concrete, so there is certain similarity that can be problematic. In the next section it will be shown that there is not such a problem for double-muon events.

Final yields

As in previous section, we show here the effect of every single cut being applied on simulated data, see Table 3.3. This time it contains absolute numbers of events instead of percentages since there is a very few events passing cuts. The cross section is, however, much higher than the one of $H \rightarrow \tau\tau$ so even a few events passing cuts is a problem. The overall number of simulated events is ten thousand.

Table 3.3: Yields of $\gamma\gamma \to ee$ cut by cut.

	FD 420+420 m			**FD 220+420 m**		
Cut	**hh**	**hl**	**ll**	**hh**	**hl**	**ll**
Identified	2	1466	1361	2	1466	1361
Acceptance	0	83	161	0	31	16
p_T(lepton)	–	9	117	–	22	16
η(lepton)	–	9	117	–	22	16
p_T(jet)	0	9	–	0	22	–
η(jet)	0	9	–	0	22	–
$\Delta\phi(jj)$	0	–	–	0	–	–
Mass Window	0	1	3	0	1	1
p_T(proton)	**0**	**0**	**2**	**0**	**0**	**0**

We can see that we loose most of events in forward taggers. Their efficiency in 420+420 configuration is 6.1%, for 220+420 configuration it is 1.3%.

In a Tab. 3.4 final yields and corresponding cross-sections and absolute numbers of events per 30 inverse femtobarns are presented. We can see that the acceptancies of proton taggers are much smaller than in previous CED Higgs boson production, for 420+420m configuration it is 6.1% and for 220+420m configuration 1.3%. What is important to notice here is a total cross section of exclusive $\gamma\gamma \to ee$ process: 2 pb. It is about ten thousands times higher than in CED Higgs boson production! Now, adding both FD 420+420m and 220+420m configurations together we get for final yields

$$\epsilon = 0.02\ \%, \quad \sigma_{obs} = 0.4\ \text{fb}, \quad N_{ev}/30\text{fb}^{-1} = 13.$$

Although the final yield is only 0.02% the number of events per 30 inverse femtobarns gives, due to a very high cross-section, 13 events. It is much more than in the case of CED $H \to \tau\tau$ even when we work with MSSM's enhancement factors (we got 2.5 events per 30 fb^{-1}). This whole contribution is, however, only in fully-leptonic channel of $\gamma\gamma \to ee$. Other channels give zero contributions. However, fully-leptonic channel originally was of a great interest of ours because of its unique experimental signature (only two central high p_T leptons and two forward protons). But for now it looks like that for 120 GeV Higgs boson it is completely killed.

Table 3.4: Summary of final yields along with corresponding cross-sections and absolute numbers of events per 30 fb^{-1} for $\gamma\gamma \to ee$ events.

Selection cuts	**FD 420+420 m**			**FD 220+420 m**		
	Eff. [%]	σ [fb]	**Events/ 30 fb^{-1}**	**Eff.** [%]	σ [fb]	**Events/ 30 fb^{-1}**
Generated	100 %	2000	60000	100 %	2000	60000
FD acceptance	6.1 %	122	3660	1.3 %	26	780
hh cuts	0.00 %	0.0	0	0.00 %	0.0	0
Mass Window	0.00 %	0.0	0	0.00 %	0.0	0
p_T(protons)	0.00 %	0.0	0	0.00 %	0.0	0
hl cuts	0.09 %	1.8	54	0.22 %	4.4	132
Mass Window	0.01 %	0.2	7	0.01 %	0.2	7
p_T(protons)	0.00 %	0.0	0	0.00 %	0.0	0
ll cuts	1.17 %	23.4	702	0.16 %	3.2	96
Mass Window	0.03 %	0.6	18	0.01 %	0.2	7
p_T(protons)	0.02 %	0.4	12	0.00 %	0.0	0
Overall	**0.02 %**	**0.4**	**12**	**0.00 %**	**0.0**	**0**

3.3.2 Exclusive $\gamma\gamma \to \mu^+\mu^-$ production

Properties of scattered protons

Given the energy range we are in, there is no reason to expect any differencies in basic distribution plots for scattered protons compared to exclusive $\gamma\gamma \to ee$ process. The same is valid for $\gamma\gamma \to \tau^+\tau^-$ discussed in next section.

Properties of reconstructed muons

Plots of basic kinematic variables, transverse momentum and pseudorapidity, are shown in Figure 3.16. The p_T range of muons is similarly to electrons from previous section very soft. This time, however, the efficiency of muon reconstruction is practically without any change to the one from $H \to \tau\tau$ studies. For efficiencies ϵ and purities P we get

$$\epsilon = 71\%,\ P = 81\%.$$

Also, contrary to the previous background process, there is in fact no problem with misidentification of muons by electrons or tauons. Out of ten thousands event (i.e. twenty thousands of muons on generator level) there are only seven reconstructed electrons and forty-three reconstructed tau-jets. This behavior is as expected since muons have a very unique signature from detector point of view.

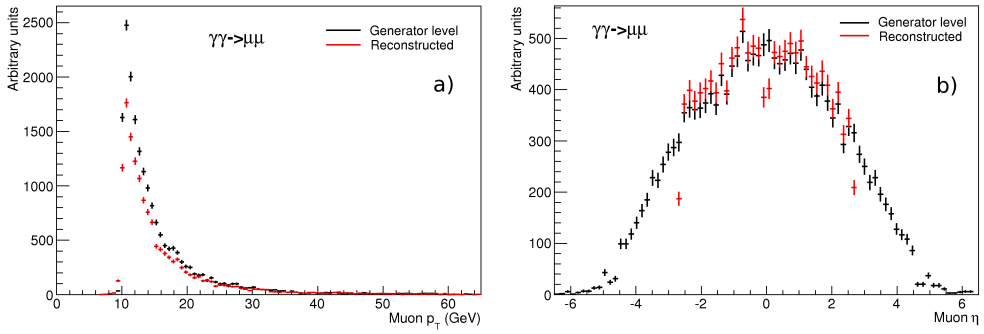

Figure 3.16: Distributions of reconstructed (red line) and generator-level (black line) muons: a) transverse momentum, b) pseudorapidity

Final yields

Table 3.5 contains again cut-flow information, i.e. numbers of passing events cut by cut. The overall number of $\gamma\gamma \to \mu\mu$ is again ten thousands.

Table 3.5: Yields of $\gamma\gamma \to \mu\mu$ cut by cut.

	FD 420+420 m			**FD 220+420 m**		
Cut	**hh**	**hl**	**ll**	**hh**	**hl**	**ll**
Identified	0	3	5640	0	3	5640
Acceptance	0	0	585	0	0	69
p_T(lepton)	–	0	572	–	0	69
η(lepton)	–	0	568	–	0	61
p_T(jet)	0	0	–	0	0	–
η(jet)	0	0	–	0	0	–
$\Delta\phi(jj)$	0	–	–	0	–	–
Mass Window	0	0	5	0	0	7
p_T(proton)	**0**	**0**	**1**	**0**	**0**	**1**

In a Tab. 3.6 final yields and corresponding cross-sections and absolute numbers of events per 30 inverse femtobarns are presented. We can see that the acceptancies as well as cross-section are the same as for $\gamma\gamma \to ee$ process. Now, adding both FD 420+420m and 220+420m configurations together we get for final yields

$$\epsilon = 0.02\ \%, \quad \sigma = 0.4\ \text{fb}, \quad N_{ev}/30\text{fb}^{-1} = 14.$$

Again, as in $\gamma\gamma \to ee$ case we can observe that the whole contribution of this background process is coming from fully-leptonic channel.

Table 3.6: Summary of final yields along with corresponding cross-sections and absolute numbers of events per 30 fb^{-1} for $\gamma\gamma \to \mu\mu$ events.

	FD 420+420 m			**FD 220+420 m**		
Selection cuts	**Eff.** [%]	σ [**fb**]	**Events/ 30 fb^{-1}**	**Eff.** [%]	σ [**fb**]	**Events/ 30 fb^{-1}**
Generated	100 %	2000	60000	100 %	2000	60000
FD acceptance	6.1 %	122	3660	1.3 %	26	780
hh cuts	0.00 %	0.0	0	0.00 %	0.0	0
Mass Window	0.00 %	0.0	0	0.00 %	0.0	0
p_T(protons)	0.00 %	0.0	0	0.00 %	0.0	0
hl cuts	0.00 %	0.0	0	0.00 %	0.0	0
Mass Window	0.00 %	0.0	0	0.00 %	0.0	0
p_T(protons)	0.00 %	0.0	0	0.00 %	0.0	0
ll cuts	5.68 %	113.6	3408	0.61 %	13.6	407
Mass Window	0.05 %	1.0	30	0.07 %	1.4	42
p_T(protons)	0.01 %	0.2	7	0.01 %	0.2	7
Overall	**0.01 %**	**0.2**	**7**	**0.01 %**	**0.2**	**7**

3.3.3 Exclusive $\gamma\gamma \to \tau^+\tau^-$ production

Properties of reconstructed tau-jets

The transverse momentum spectrum and pseudorapidity distribution are shown in Fig. 3.17.

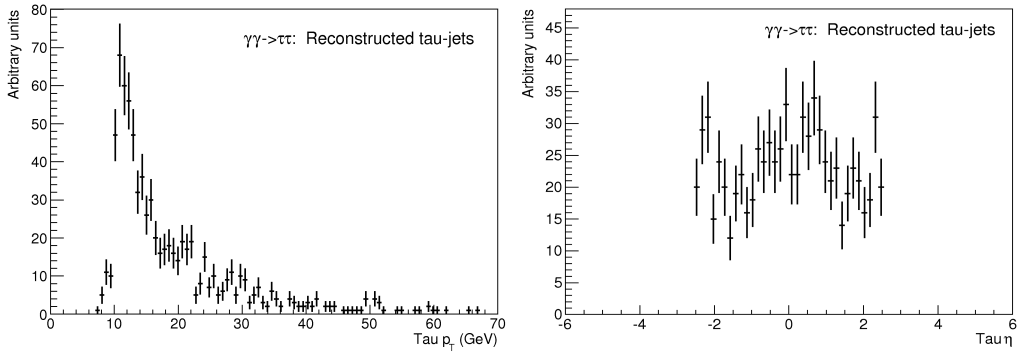

Figure 3.17: Distributions of reconstructed tau-jets: a) transverse momentum, b) pseudorapidity

Properties of reconstructed leptons

As in the $H \to \tau\tau$ case, tauons can decay either in a hadronic way (i.e. tau-jets) or into lighter leptons (electron or muon plus additional neutrino). This decay scheme suggests that electrons and muons should have softer spectrum. This is confirmed in Fig. 3.18. Majority of these leptons are apparently below 10 GeV so the standard kinematic cuts defined in Section 3.1 should be able to stop most of them.

Final yields

Finally, the evaluation of particular cuts is possible to see from cut-flow table 3.7. The overall number of $\gamma\gamma \to \tau\tau$ events is again ten thousands. Apparently, the definition of mass window is crucial here for effective suppresion of this background process.

In a Tab. 3.8 final yields and corresponding cross-sections and absolute numbers of events per 30 inverse femtobarns are presented. The cross-section is this time slightly lower than in $\gamma\gamma \to ee/\mu\mu$ processes. We can see that this background process gives zero contributions after applying all cuts for all channels, including the fully-leptonic one.

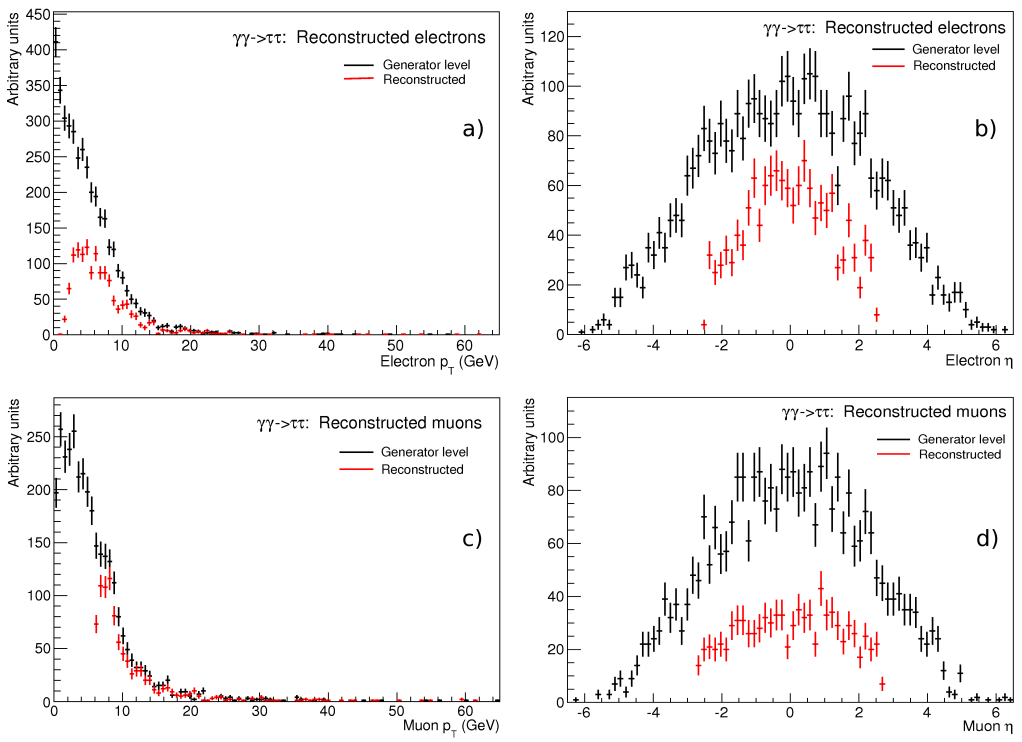

Figure 3.18: Distributions of reconstructed (red line) and generator-level (black line) leptons: a,c) transverse momenta, b,d) pseudorapidities

Table 3.7: Yields of $\gamma\gamma \to \tau\tau$ cut by cut.

	FD 420+420 m			**FD 220+420 m**		
Cut	**hh**	**hl**	**ll**	**hh**	**hl**	**ll**
Identified	37	204	165	37	204	165
Acceptance	7	46	20	7	11	9
p_T(lepton)	–	6	2	–	5	7
η(lepton)	–	6	2	–	5	7
p_T(jet)	3	5	–	7	5	–
η(jet)	3	5	–	7	5	–
$\Delta\phi(jj)$	3	–	–	6	–	–
Mass Window	0	0	0	0	1	1
p_T(proton)	**0**	**0**	**0**	**0**	**0**	**0**

Table 3.8: Summary of final yields along with corresponding cross-sections and absolute numbers of events per 30 fb^{-1} for $\gamma\gamma \to \tau\tau$ events.

Selection cuts	**FD 420+420 m**			**FD 220+420 m**		
	Eff. [%]	σ [fb]	**Events/ 30 fb^{-1}**	**Eff.** [%]	σ [fb]	**Events/ 30 fb^{-1}**
Generated	100 %	1963	58890	100 %	1963	58890
FD acceptance	6.1 %	120	3592	1.3 %	26	766
hh cuts	0.03 %	0.6	18	0.06 %	1.2	35
Mass Window	0.00 %	0.0	0	0.00 %	0.0	0
p_T(protons)	0.00 %	0.0	0	0.00 %	0.0	0
hl cuts	0.05 %	1.0	29	0.05 %	1.0	29
Mass Window	0.00 %	0.0	0	0.01 %	0.2	6
p_T(protons)	0.00 %	0.0	0	0.00 %	0.0	0
ll cuts	0.02 %	0.4	12	0.07 %	1.4	41
Mass Window	0.00 %	0.0	0	0.01 %	0.2	6
p_T(protons)	0.00 %	0.0	0	0.00 %	0.0	0
Overall	**0.00 %**	**0.0**	**0**	**0.00 %**	**0.0**	**0**

3.3.4 Exclusive gluon-gluon fusion process

Another background source is the exclusive production of $gg \rightarrow gg$. These samples can be generated by ExHuME MC generator and are already simulated as official ATLAS datasets (for 10 TeV CMS energy and two different transverse energies of produced gluons, 35 GeV and 17 GeV):

mc08.106065.ExhumeGG_Et35.merge.AOD.e386_s495_r635_t53
(twenty thousands events)
mc08.106064.ExhumeGG_Et17.merge.AOD.e386_s495_r635_t53
(thirty thousands events)

Properties of diffractive protons

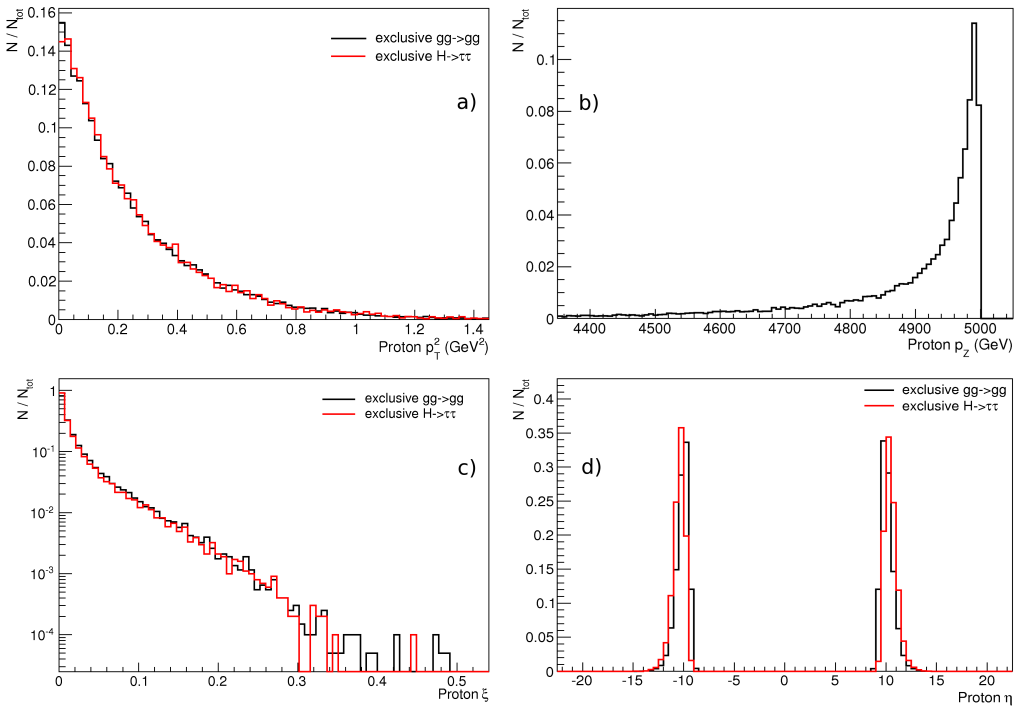

Figure 3.19: Distributions of diffractive protons: a) transverse momentum squared, b) momentum projection to beam axis, c) fractional momentum loss (see Section 1.5), d) pseudorapidity. Distributions are normalized to the overall number of events, i.e. 20k for E_T =35 GeV and 30k for E_T =17 GeV.

In Fig. 3.19 basic kinematic distributions for diffractive protons of exclusive gluon-gluon fusion in comparison with exclusive $H \rightarrow \tau\tau$ are presented. One can see that alghough gg fusion samples are generated for 10 TeV CMS energy,(in contrast with 14 TeV of $H \rightarrow \tau\tau$) we still get practially identical distributions. Figure 3.20 depicts missing mass distribution. As in

the exclusive $\gamma\gamma$ production of di-leptons, the missing mass window will remove most of these background events.

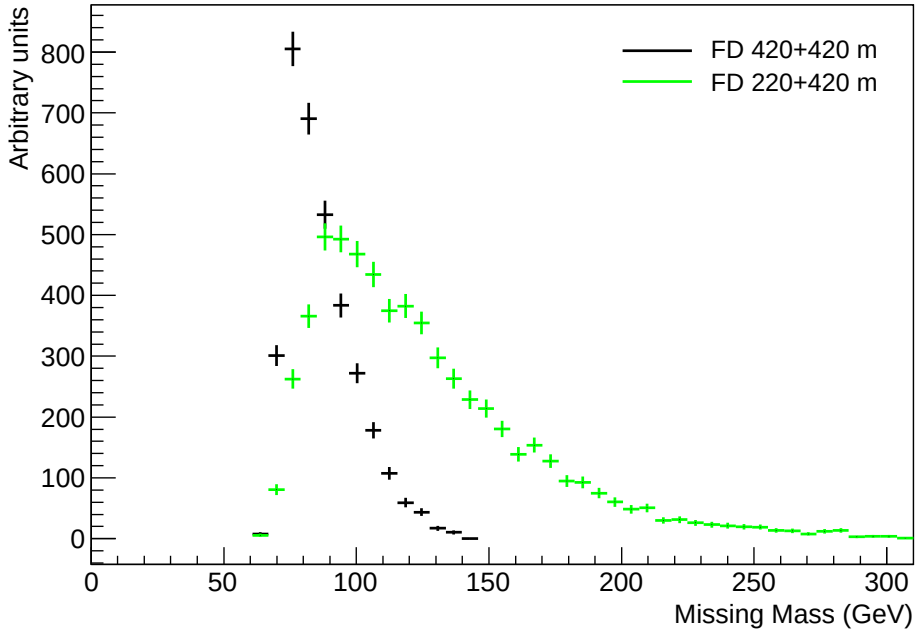

Figure 3.20: Missing mass distribution of exclusive gg fusion process for E_T = 35 GeV.

Properties of reconstructed tau-jets

Basic distribution plots for tau-jets are in Fig. 3.21. Transverse momenta are apparently in smaller ranges for 17 GeV samples than for 35 GeV samples. Pseudorapidities have the usual expected shape.

Properties of reconstructed leptons

Basic distributions of reconstructed leptons are shown in Fig. 3.22. They are apparently in very small p_T range. It is surprising that there is so much identified leptons (mostly electrons). Out of twenty thousands events (samples with $E_T = 35$ GeV) there are 1210 electrons and 227 muons. This feature certainly needs further investigation. It completely kills the fully-leptonic channel of $H \to \tau\tau$ as we will see in 'Final yields' subsection.

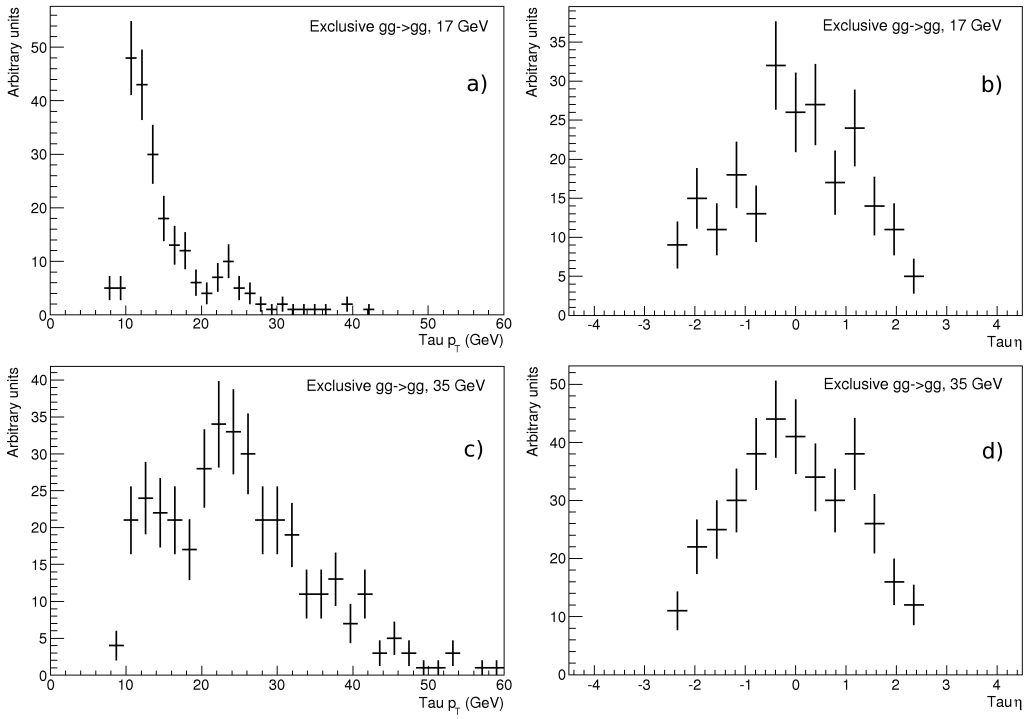

Figure 3.21: Distributions of reconstructed tau-jets: transverse momenta and pseudorapidities for $E_T = 17$ GeV are in a-b), for $E_T = 35$ GeV in c-d).

Final yields

In Tables 3.9 and 3.10 there are yields of exclusive $gg \to gg$ cut by cut for $E_T = 35$ GeV and $E_T = 17$ GeV. In a Tab. 3.11 final yields and corresponding cross-sections and absolute numbers of events per 30 inverse femtobarns for $E_T = 35$ GeV are presented (equivalent table for 17 GeV is not necessary since all columns would be zeros, see Tab. 3.10). Cross sections of this background process is really huge compared to the previous ones (CED $H \to \tau\tau$ as well as $\gamma\gamma$ fusions), 198 pb! Although there is only one fully-leptonic event surviving all cuts (for $E_T = 35$ GeV) out of twenty thousands, it makes 297 events per 30 fb^{-1} which is around hundred time more than contribution of whole CED $H \to \tau\tau$.

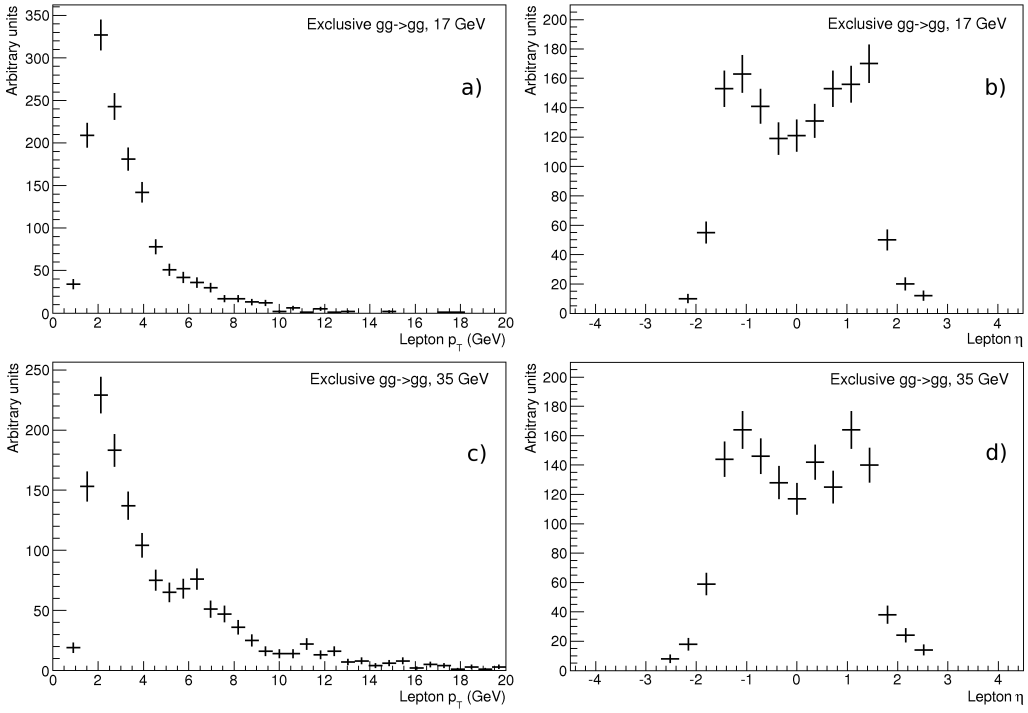

Figure 3.22: Distributions of reconstructed leptons: transverse momenta and pseudorapidities for $E_T = 17$ GeV are in a-b), for $E_T = 35$ GeV in c-d).

Table 3.9: Yields of $gg \to gg$ cut by cut; $E_T = 35$ GeV.

	FD 420+420 m			**FD 220+420 m**		
Cut	**hh**	**hl**	**ll**	**hh**	**hl**	**ll**
Identified	2	32	55	2	32	55
Acceptance	1	7	12	1	8	24
p_T(lepton)	–	0	0	–	1	2
η(lepton)	–	0	0	–	1	2
p_T(jet)	1	0	–	1	1	–
η(jet)	1	0	–	1	1	–
$\Delta\phi(jj)$	0	–	–	0	–	–
Mass Window	0	0	0	0	0	1
p_T(proton)	**0**	**0**	**0**	**0**	**0**	**1**

Table 3.10: Yields of $gg \to gg$ cut by cut; $E_T = 17$ GeV.

	FD 420+420 m			**FD 220+420 m**		
Cut	**hh**	**hl**	**ll**	**hh**	**hl**	**ll**
Identified	1	12	48	1	12	48
Acceptance	1	1	16	0	0	5
p_T(lepton)	–	0	0	–	0	0
η(lepton)	–	0	0	–	0	0
p_T(jet)	0	0	–	0	0	–
η(jet)	0	0	–	0	0	–
$\Delta\phi(jj)$	0	–	–	0	–	–
Mass Window	0	0	0	0	0	0
p_T(proton)	**0**	**0**	**0**	**0**	**0**	**0**

Table 3.11: Summary of final yields along with corresponding cross-sections and absolute numbers of events per 30 fb^{-1} for exclusive $gg \to gg$ events; $E_T = 35$ GeV.

Selection cuts	**FD 420+420 m**			**FD 220+420 m**		
	Eff. [%]	σ [**fb**]	**Events/ 30 fb^{-1}**	**Eff.** [%]	σ [**fb**]	**Events/ 30 fb^{-1}**
Generated	100 %	198000	5940000	100 %	198000	5940000
FD acceptance	17 %	33660	1009800	30 %	59400	1782000
hh cuts	0.00 %	0.0	0	0.00 %	0.0	0
Mass Window	0.00 %	0.0	0	0.00 %	0.0	0
p_T(protons)	0.00 %	0.0	0	0.00 %	0.0	0
hl cuts	0.00 %	0.0	0	0.005 %	9.9	297
Mass Window	0.00 %	0.0	0	0.00 %	0.0	0
p_T(protons)	0.00 %	0.0	0	0.00 %	0.0	0
ll cuts	0.00 %	0.0	0	0.01 %	19.8	594
Mass Window	0.00 %	0.0	0	0.005 %	9.9	297
p_T(protons)	0.00 %	0.0	0	0.005 %	9.9	297
Overall	**0.00 %**	**0.0**	**0**	**0.005 %**	**9.9**	**297**

3.4 Final remarks

Except exclusive $\gamma\gamma$ fusion process and exclusive production of high E_T gluons there is one more source of background that has not been discussed yet - di-jet events combined with pile-up (i.e. multiple interactions per bunch crossing). The reason is that these samples were not available in time of writing this thesis and thus the private production was not possible (hundreds thousands of events needed, not to mention issues with pile-up generation and simulation).

Concearning backgrounds processed in this thesis, one thing is necessary to mention: due to their very high cross sections (compared to exclusive $H \rightarrow \tau\tau$ events) the size of samples (ten thousands for $\gamma\gamma$ fusion and from twenty to thirty thousands for high E_T gluons production) is very unsatisfactory. For higher reliability of these results analysis with higher statistics has to be performed.

As we have seen, there are still some issues that need to be examined and some tasks that need to be performed:

- higher statistics samples have to be used for all background processes
- last significant source of background, overlapping pile-up events, has tobe investigated
- there are also some detector-level issues that need further studies (unexpectedly high number of surviving background events in the fully-leptonic channel - especially in the case of CED $gg \rightarrow gg$ where gluon jets are misidentified as electrons; also, the di-electron final state in the $\gamma\gamma \rightarrow ee$ events is sometimes misidentified as tau-jets)
- some work on tuning selection/rejection cuts has to be done
- investigatation of other Higgs boson masses from 100 up to 300 GeV is necessary for completion of exclusive $H \rightarrow \tau\tau$ studies

Chapter 4

Conclusion

This master thesis presents studies of central exclusive diffractive production of Higgs boson of 120 GeV mass in tau-channel, $H \rightarrow \tau\tau$, based on Monte Carlo generation and ATLAS detector response simulation. It is aimed as a study of Minimal Supersymmetric Standard Model Higgs boson since enhancement factors for cross-section of this process (very low in Standard Model) are expected, as shown in Section 1.8.

First task in this study was to develop a procedure for identification of three types of $\tau\tau$ decay channels (fully-hadronic, semi-leptonic and fully-leptonic) just from detector-level information. Also, a proper combination of software settings for final identification of reconstructed particles (tau-jets, electrons and muons) had to be chosen. As a next task, a thorough study of properties of reconstructed particles and identified events was done in order to get understanding of these unique processes. Finally, a preselection of appropriate cuts on reconstructed particles was done.

Apart from analysis of CED $H \rightarrow \tau\tau$ itself, background processes have also been studied: exclusive QED $\gamma\gamma$ fusion process producing pairs of leptons (electrons, muons and tauons) and CED gluon-gluon fusion process producing two jets. A convenient choice of selection cuts was necessary in order to suppress these background processes as much as possible. The last background process, di-jet events combined with pile-up, is not included in this study since in time of writing this thesis the appropriate datasets were not available.

As it turned out, two tauons in final state produced in CED production of 120 GeV Higgs boson have unique experimental signatures. First, given the kinematics, hadronic tau decays have in general higher transverse momenta (20-50 GeV), compared e.g. to tau-candidates expected to be seen in the early LHC data. As a consequence, the tau-jet identification procedure

is reasonably high (90% for Loose method used in this analysis). Similarly, spectrum of reconstructed electrons and muons is also in higher transverse momenta ranges (although not so high as tau-jets because of additional neutrinos carrying away certain amount of energy) compared to those coming from background processes mentioned above. For electrons we also observe higher reconstruction efficiency, for muons it practically does not change. Finally, it turned out that misidentification of gluonic jets with tau-jets is practically none and preliminary studies of di-jet events (from Pythia generation) combined with pile-up suggest that similar behavior is to be expected in this case as well. This feature is given by unique tau-jet properties.

Results of this analysis suggest that CED $H \rightarrow \tau\tau$ process could be measurable in MSSM in the fully-hadronic and semi-leptonic modes: for a moderate MSSM enhancement factor of 10, one can expect 1.3 events per integrated luminosity of 30 fb^{-1} with a negligible background. The fully-leptonic channel seems to be dominated by background events which is not well understood yet.

It is necessary to stress that the obtained results are still preliminary and that there is a room for improvement. In particular, higher statistics samples have to be used for all background processes and some work on tuning the selection/rejection cuts has to be done. There are also a few outstanding issues at detector level that need to be studied and better understood. Also, very importantly, the last significant source of background, the overlap of pile-up events, has to be investigated. A plan is to perform a complete mass scan from masses of 100 up to 300 GeV.

Bibliography

[1] M.J.Herrero, *The Standard Model*, arXiv:hep-ph/9812242v1, 1998

[2] Horejsi J., *Fundamentals of electroweak theory*, The Karolinum Press, Charles University in Prague, 2002

[3] Abdelhak Djouadi, *The Anatomy of electro-weak symmetry breaking. I: The Higgs boson in the standard model*, arXiv:hep-ph/0503172

[4] ALEPH, DELPHI, L3 and OPAL Collaborations, *The LEP Working Group for Higgs Boson Searches*, Phys. Lett. B565 (2003) 61, hep-ex/0306033

[5] M. Gomez-Bock, M. Mondragón, M. Mühlleitner, M. Spira, P.M. Zerwas, *Concepts of Electroweak Symmetry Breaking and Higgs Physics*, arXiv:0712.2419v1 [hep-ph]

[6] Abdelhak Djouadi, *The Anatomy of electro-weak symmetry breaking. II: The Higgs bosons in the minimal supersymmetric model*, arXiv:hep-ph/0503173

[7] Barone V., Predazzi E., *High-Energy Particle Diffraction*, Springer, 2002

[8] P.D.B. Collins, *An Introduction to Regge Theory and High-Energy Physics*, Cambridge University Press, Cambridge, 1977.

[9] E.A. Kuraev, L.N. Lipatov and V.S. Fadin, Sov. Phys. JETP 44 (1976) 443; ibid. 45 (1977) 199;
I. I. Balitsky and L.N. Lipatov, Sov. J. Nucl. Phys. 28 (1978) 822.

[10] M. Wüsthoff and A.D. Martin, J. Phys. G 25 (1999) R309 arXiv:hep-ph/9909362;
J. R. Forshaw and D. A. Ross, *Quantum chromodynamics and the pomeron*, Cambridge Lect. Notes Phys. 9 (1997) 1;

[11] A.B. Kaidalov, V.A. Khoze, A.D. Martin and M.G. Ryskin, *Central exclusive diffractive production as a spin-parity analyser: From Hadrons to Higgs*, arXiv:hep-ph/0307064

[12] V.A. Khoze, A.B. Kaidalov, A.D.Martin, M.G. Ryskin and W.J. Stirling, *Diffractive processes as a tool for searching for new physics*, arXiv:hep-ph/0507040

[13] V.A. Khoze, A.D Martin and M.G. Ryskin, *Diffractive Higgs production: Myths and reality*, arXiv:hep-ph/0207313

[14] B.E. Cox et al., Eur.Phys.J.C45:401-407,2006, arXiv:hep-ph/0505240

[15] S. Heinemeyer, V.A. Khoze, M.G. Ryskin, W.J. Stirling M. Tasevsky and G. Weiglein, Eur. Phys. J. C 53, 231-256 (2008)

[16] Particle Data Group, Particle Physics Booklet, 2002,http://pdg.lbl.gov

[17] M. Albrow et al., *Prospects for diffractive and forward physics at the LHC*, CERN-LHCC-2006-039, CERN-LHCC-G-124, CERN-CMS-NOTE-2007-002, Dec 2006

[18] E. Boonekamp, T. Kúcs, *DPEMC: A Monte-Carlo for Double Diffraction*, arXiv:hep-ph/0312273

[19] V. A. Petrov, R. A. Ryutin, A. E. Sobol, *EDDE Monte Carlo event generator*, arXiv:hep-ph/0409180.

[20] T. Sjostrand, L. Lonnblad and S. Mrenna, arXiv:hep-ph/0108264

[21] J. Monk and A. Pilkington, *ExHuME: A Monte Carlo Event Generator for Exclusive Diffraction*, arXiv:hep-ph/0502077

[22] V. A. Khozehe, A. D Martin and M. G. Ryskin, *Prospects for new physics observations in diffractive processes at the LHC and Tevatron*, arXiv:hep-ph/0111078

[23] A. Bialas and P. V. Landshoff, Phys. Lett. B B256, 540 (1991)

[24] V. A. Petrov and R. Ryutin, Eur. Phys. Journ C36, 509 (2004)

[25] S. Heinemeyer, V.A. Khoze, M.G. Ryskin, W.J. Stirling, M. Tasevsky and G. Weiglein, *Studying the MSSM Higgs sector by forward proton tagging at the LHC*, arXiv:0708.3052v2 [hep-ph] 1. Oct. 2007

[26] M.G. Albrow et al. [FP420 Collab.], arXiv:0806.0302[hep-ex]

[27] M. Boonekamp, V. Juranek, O. Kepka, C. Royon, Forward Physics Monte Carlo
H. Jung *et al.*, *Proceedings of the workshop: HERA and the LHC workshop series on the implications of HERA for LHC physics*, arXiv:0903.3861 [hep-ph].

[28] ATHENA framework site,
https://twiki.cern.ch/twiki/bin/view/Atlas/AthenaFramework

[29] Gaudi project site, http://proj-gaudi.web.cern.ch/proj-gaudi

[30] Nuclear Instruments and Methods in Physics Research, A 506 (2003) 250-303

[31] ElectronGamma Conbined Performance Group site,
https://twiki.cern.ch/twiki/bin/view/AtlasProtected/ElectronGamma

[32] Muon Combined Performance Working Group site,
https://twiki.cern.ch/twiki/bin/view/AtlasProtected/MuonPerformance

[33] ATLAS CSC Note, *Identification of hadronic τ decays with ATLAS detector*, ATLAS-PHYS-INT-2008-003

[34] Particle Data Group, Particle Physics Booklet, 2006, http://pdg.lbl.gov